

Winter 2013

Laser assisted milling of difficult to machine materials

Gary Kent Hedberg
Purdue University

Follow this and additional works at: https://docs.lib.purdue.edu/open_access_theses



Part of the [Mechanical Engineering Commons](#)

Recommended Citation

Hedberg, Gary Kent, "Laser assisted milling of difficult to machine materials" (2013). *Open Access Theses*. 729.
https://docs.lib.purdue.edu/open_access_theses/729

This document has been made available through Purdue e-Pubs, a service of the Purdue University Libraries. Please contact epubs@purdue.edu for additional information.

PURDUE UNIVERSITY
GRADUATE SCHOOL
Thesis/Dissertation Acceptance

This is to certify that the thesis/dissertation prepared

By Gary Kent Hedberg

Entitled

LASER ASSISTED MILLING OF DIFFICULT TO MACHINE MATERIALS

For the degree of Master of Science in Mechanical Engineering

Is approved by the final examining committee:

Yung C. Shin

Chair

Eric Kvam

Galen King

To the best of my knowledge and as understood by the student in the *Research Integrity and Copyright Disclaimer (Graduate School Form 20)*, this thesis/dissertation adheres to the provisions of Purdue University's "Policy on Integrity in Research" and the use of copyrighted material.

Approved by Major Professor(s): Yung C. Shin

Approved by: David C. Anderson

Head of the Graduate Program

12/18/13

Date

LASER ASSISTED MILLING OF DIFFICULT TO MACHINE MATERIALS

A Thesis

Submitted to the Faculty

of

Purdue University

by

Gary Kent Hedberg

In Partial Fulfillment of the

Requirements for the Degree

of

Master of Science in Mechanical Engineering

May 2014

Purdue University

West Lafayette, Indiana

For my parents

ACKNOWLEDGEMENTS

I am extremely grateful for the help I have received while working on this research. I want to thank my dad, whose constant enthusiasm and encouragement helped me through all the ups and downs in the work. I am so grateful for the support that he gives me in so many aspects of my life. I also want to thank Dr. Yung Shin for his patience and guidance as the work progressed. I am grateful for the times when he could offer counsel that changed my perspective and help me to see my way forward more clearly. I would also like to thank Dr. Eric Kvam and Dr. Galen King for serving on my committee.

I would also like to give thanks to Mike Sherwood and Adam Krichbaum for their expertise and advice. I am so grateful for their assistance in my work.

I appreciate the time and friendship my labmates have offered along the way. I am grateful for Hongtao Ding, who helped me improve by providing so much of his time and advice. I am also grateful for Mike Wilson who has a great perspective on life and advice on work. I have also appreciated the good discussions I have had with Neil Bailey, Nathan Toner, and Wenda Tan.

I am so very grateful for the blessing of a wonderful and supportive family. I want to thank each and every one of them for their love and the fun we have together. I am so grateful for how they remind me of what is most important in life.

TABLE OF CONTENTS

	Page
LIST OF TABLES	vii
LIST OF FIGURES	ix
LIST OF SYMBOLS.....	xiii
ABSTRACT	xv
CHAPTER 1. INTRODUCTION.....	1
1.1 Rationale	1
1.2 Material Properties of Titanium Alloys	3
1.3 Machining of Titanium Alloys	8
1.4 Literature Review of Laser-Assisted Machining.....	13
1.4.1 Laser-Assisted Turning	13
1.4.2 Laser-Assisted Milling	15
1.5 Objectives.....	17
CHAPTER 2. EXPERIMENTAL SETUP AND THERMAL MODELING	19
2.1 Experimental Setup	19
2.2 Ti-64 Thermal Modeling and Validation	26
2.2.1 Mathematical Formulae and Assumptions	27
2.2.2 Temperature Dependent Properties	30
2.2.3 Laser Absorptivity.....	31
2.2.4 Statistical Modeling for Temperature Prediction.....	38
2.2.5 Temperature Modeling of Material in Removal Zone	44

	Page
CHAPTER 3. LASER-ASSISTED MILLING OF TI-64	46
3.1 Ti-64 Grade 5	46
3.1.1 Experimental Design and Procedure.....	46
3.1.2 Experimental Results and Discussion	48
3.1.2.1 Cutting Force.....	48
3.1.2.2 Tool Wear Analysis	53
3.1.2.3 Microstructural Analysis	59
3.1.3 Economic Analysis	69
3.2 Ti-64 ELI grade 23.....	73
3.2.1 Experimental Design and Procedure.....	73
3.2.2 Experimental Results and Discussion	73
3.2.2.1 Cutting Force.....	73
3.2.2.2 Tool Wear Analysis	76
3.2.2.3 Microstructural Analysis	81
3.2.3 Economic Analysis	90
CHAPTER 4. LASER-ASSISTED MILLING – COMPLEX CONTOURING.....	94
4.1 System Design	94
4.2 System Integration and Experimental Setup	94
4.2.1 System Integration	94
4.2.2 Experimental Setup.....	96
4.3 Experimental Results.....	97
CHAPTER 5. CONCLUSIONS AND RECOMMENDATIONS	99
5.1 Conclusions.....	99

	Page
5.2 Recommendations.....	101
LIST OF REFERENCES	103
VITA	109

LIST OF TABLES

Table	Page
Table 1.1: Ti-64 grade 5 workpiece with AMS 4911 specifications.....	6
Table 1.2: Ti-64 ELI grade 23 workpiece with AMS 4931 specifications.	6
Table 1.3: Ti-64 grade 5 mechanical properties for AMS 4911.	6
Table 1.4: Ti-64 ELI grade 23 mechanical properties for AMS 4931.	7
Table 1.5: Machining parameters for Ti-64.....	11
Table 2.1: Cutting tool parameters.	23
Table 2.2: IR camera characteristics.	24
Table 2.3: Temperature dependent property equations for Ti-64.	31
Table 2.4: IR camera settings.....	33
Table 2.5: Heating test conditions and results.....	37
Table 2.6: Constants used in thermal model.	39
Table 2.7: Thermal model conditions.....	40
Table 3.1: Cutting speed and force results for traditional experiments.	49
Table 3.2: Experimental design for LAML of Ti-64.....	50
Table 3.3: Invariant laser parameters.	50
Table 3.4: LAML experimental matrix and cutting force results.	52
Table 3.5: Tool Wear Experimental Parameters.....	53
Table 3.6: Optimized cutting speed from Taylor tool life equations.	70

Table	Page
Table 3.7: Experimental Design for LAML of Ti-64.....	74
Table 3.8: Experimental Matrix and Results of Milling of Ti-64.....	75
Table 3.9: Tool Wear – experimental parameters.....	78
Table 3.10: Optimized cutting speed based on Taylor tool life equations – Ti-64 ELI milling.....	92
Table 4.1: Experimental Design for Complex Contouring Tests.	97

LIST OF FIGURES

Figure	Page
Figure 1.1: Generic isomorphous binary phase diagram of titanium (Zhecheva et al., 2005).	5
Figure 1.2: Percentage of ultimate tensile strength as a function of temperature for Ti-64 (Air Force Materials Laboratory, 1972).....	8
Figure 2.1: Laser head degrees of freedom and laser spot setup.	21
Figure 2.2: General machining setup for LAML (top view).....	22
Figure 2.3: Prismatic thermal model boundary conditions.	27
Figure 2.4: Specific heat and thermal conductivity of Ti-64 (Touloukian, 1970)..	30
Figure 2.5: Plot of emissivity vs. Ti-64 surface temperature at 8500 nm wavelength for IR Camera from literature (Hahn et al., 2006) and fiber laser heating experiments.	33
Figure 2.6: IR camera image of workpiece surface during laser heating.	34
Figure 2.7: IR camera temperature results and thermal model temperature prediction for maximum workpiece temperature.	36
Figure 2.8: Absorptivity validation for Ti-64 grade 5.	38
Figure 2.9: Thermal model example output for LAML of Ti-64.	41
Figure 2.10: Thermal model simulation results for LAML temperature prediction.	44

Figure	Page
Figure 2.11: Images for curved and straight T_{mr-ave} calculations.....	45
Figure 3.1: Machining coordinate system based on dynamometer.....	47
Figure 3.2: Cutting force measurements from traditional machining.....	49
Figure 3.3: Experimental cutting force during multiple tool rotations.	51
Figure 3.4: Average peak cutting force results with error bars for one standard deviation.	52
Figure 3.5: Tool wear images for CONV-B with KC520 insert.	55
Figure 3.6: Tool wear images for LAML-B at 500 °C T_{mr-ave} with KC520 insert...	56
Figure 3.7: Ti-64 tool wear for traditional milling and LAML using a KC520 insert.	57
Figure 3.8: Taylor tool life equations for Ti-64.	59
Figure 3.9: Ti-64 optical microscope images from cross-sectioned samples etched with Kroll's reagent at 200x after traditional machining (a) and LAML (b).	60
Figure 3.10: SEM images of etched Ti-64 sample at 1,000x after traditional machining (a) and LAML (b).	61
Figure 3.11: Temperature profile in workpiece with laser scan and feed into page.	63
Figure 3.12: XRD analysis for milling Ti-64.....	64
Figure 3.13: Ti-64 surface hardness results for the as-received material, Conv-C at 50 m/min and LAML-C at 75 m/min.	65
Figure 3.14: Microhardness results for Conv-C and LAML-C.	67

Figure	Page
Figure 3.15: Residual Stress measurement for Ti-64 after Conv-C and LAML-C for machining direction (a) and feed direction (b).	68
Figure 3.16: Cost of producing one part based on Taylor tool life equations.	71
Figure 3.17: Machining costs for optimized traditional machining and LAML.	71
Figure 3.18: Material removal rates for traditional machining and LAML.	72
Figure 3.19: Average Peak Cutting Force Results – error bars for one standard deviation.	75
Figure 3.20: ELI Tool Wear – 725M Insert.....	79
Figure 3.21: Taylor tool life equations and experimental data for Ti-64 ELI.....	81
Figure 3.22: Ti-64 ELI Optical Microscope images from cross-sectioned samples etched with Kroll’s reagent at 200x after traditional machining (a) and LAML (b).	83
Figure 3.23: SEM Images of etched Ti-64 sample at 1,000x after traditional machining (a) and LAML (b).	84
Figure 3.24: XRD analysis for milling Ti-64.....	85
Figure 3.25: Ti-64 ELI surface hardness results for the as-received material, traditional milling at 50 m/min, and LAML at 75 m/min (error bars for the range of data).	86
Figure 3.26: MicroHardness results for traditional machining at 50 m/min and LAML at 75 m/min.	88

Figure	Page
Figure 3.27: Residual Stress measurement for Ti-64 ELI after traditional machining at 50 m/min and LAML at 75 m/min for the machining direction (a) and feed direction (b).....	89
Figure 3.28: Cost of producing one part based on Taylor tool life equations.	91
Figure 3.29: Economic Summary for optimized cutting conditions – Ti-64 ELI machining.	92
Figure 4.1: 4-Axis OAC hardware layout.	95
Figure 4.2: LAML Contouring Path for Experiments with One Direction Machining.	96

LIST OF SYMBOLS

Symbol	
α_n	absorptivity of a Nd:Yag laser on a Ti-64 workpiece
α_f	absorptivity of the fiber laser on a Ti-64 workpiece
ε	emissivity of the workpiece
λ	wavelength (nm)
ρ	density of the workpiece (kg/m ³)
ε	emissivity of the workpiece
C_{entry}	entry angle of the cutting tool into the workpiece (°)
C_{exit}	exit angle of the cutting tool from the workpiece (°)
c_p	specific heat (J/kg·K)
D_{oc}	depth of cut (mm)
F	feed rate (mm/min)
f	feed per tooth (mm/tooth)
k	thermal conductivity (W/m·K)
L_{angle}	angle of incidence of the laser beam onto the workpiece measured from the horizontal (°)
L_{lead}	distance between the laser spot and the tool entering workpiece material (mm)
L_{offset}	distance between the edge of the workpiece and edge of the laser (mm)

Symbol

L_{spot}	maximum size of the beam diameter onto the workpiece for the feed direction and cutting direction (mm ²)
P	laser power (W)
T_{max}	maximum temperature of the workpiece surface (°C)
$T_{\text{mr-ave}}$	average temperature of the workpiece within the cutting zone (°C)
T_{machined}	maximum temperature of workpiece surface at the depth of cut plane (°C)
$T_{\text{oxidation}}$	minimum temperature for oxidation to occur on the metal
T_{phase}	minimum temperature for phase change to occur for the metal
V	velocity of insert or cutting speed (m/min)
W_{oc}	width of cut (mm)

ABSTRACT

Hedberg, Gary K. M.S.M.E., Purdue University, May 2014. Laser-Assisted Milling of Difficult to Machine Materials. Major Professor: Yung Shin, School of Mechanical Engineering.

Titanium alloys are well known for their excellent strength to weight ratio and corrosion resistance and is highly sought after in the aerospace industry. Additionally, titanium alloys maintain a high biocompatibility for implants and other medical devices. However, these alloys are notorious for their poor machinability. As the demand for these alloys continue to increase, improved methods of manufacture must be explored.

This thesis describes Laser Assisted Milling (LAML) of Ti-6AL-4V (Ti-64) alloys, which studies localized preheating of the workpiece by a laser and characterizes the improvements to the machinability of these metals. Laser parameters are determined based on temperature prediction modeling results. Laser preheating is shown to reduce cutting force during the machining process. Machinability improvement is characterized through inspection of flank wear on the cutting tool using LAML and traditional machining methods and comparing total tool life. Systematic characterization of samples is performed using hardness measurements, scanning electron microscopy (SEM), and X-ray

diffraction (XRD) to ensure that material properties remained unaltered as a result of laser preheating.

An economic analysis is performed to characterize the cost benefit of machining using LAML while considering the additional costs associated with the laser equipment. Economic improvements are shown for the LAML process for Ti-64 alloys. A rotary axis is added to the machining equipment to overcome design constraints from the laser setup and allow for the machining of complex shapes. The feasibility of complex contouring is demonstrated for LAML with the creation of more intricate geometry being performed on a titanium workpiece.

CHAPTER 1. INTRODUCTION

1.1 Rationale

Improvements in manufactured parts result from the discovery of advanced materials and their corresponding improvements in strength, weight, wear resistance, or other properties when compared with standard materials. Increased use of advanced materials brings about a need for innovation in manufacturing techniques capable of producing quality parts both economically and rapidly. Additionally, the improved properties of new advanced materials typically require new methods of manufacturing to obtain the best results for the created component. For example, an increase in strength and heat resistance can directly result in a decrease in the life of the cutting tool during machining.

One advanced material that continues to see a wide range of applications for improved part performance is titanium. Discovered in 1791, it has only been within the last 50 years that manufacturing methods and alloying techniques have been developed that allow for the creation of titanium components. Titanium and its alloys have seen increased use in aerospace applications, as well as other areas, due to their unique properties of high strength and relatively low density. However, titanium components, while in great demand, are also well known for the difficulties they present in manufacturing. Consequently, there

exists a need for further investigation into manufacturing techniques that will improve part production speed and quality without influencing final part properties. Thermally-assisted machining has been suggested as one such potential improvement for titanium machining.

During turning and milling operations, the standard machining practice is to use a coolant to cool and lubricate the cutting tool during machining to improve tool life and surface integrity. In recent years, other methods of thermally influencing the workpiece and cutting tool have been studied to improve machinability of advanced materials. Studied methods include cryogenic cooling of the tool to improve hardness and wear resistance, and heating the workpiece to thermally soften it and improve tool performance.

The varied approaches to thermally-assisted machining will influence the tool and workpiece in different ways. Through cryogenic cooling, the temperature of the tool can be reduced, which will improve tool wear over time. Conversely, by heating the workpiece, the material is thermally softened and the cutting force required to remove material can be greatly decreased. An important aspect in both of these techniques is the precise control of the thermal effects.

Although the benefits of thermally-assisted machining have been shown experimentally, these advanced techniques need a rigorous study before they can be fully adopted into large-scale industrial practice. Consequently, the work presented in this thesis aims to characterize the general improvements that can be made during the machining of titanium alloys when heating effects are applied in order to reduce cutting forces.

1.2 Material Properties of Titanium Alloys

The many beneficial properties of titanium and its alloys have been studied and are well known, making it highly sought after in many fields, especially the aerospace and medical industries. One key advantage of this material is its high strength, which is comparable to steel, and its ability to maintain that strength at very high temperatures. Pure titanium will maintain its strength up to 600 °C while some titanium alloys can retain their strength up to 760 °C. Titanium and its alloys also have a 40% lower density than that of steel (Chandler, 1989; Air Force Materials Laboratory, 1972). These properties make titanium an excellent choice for aerospace components, which must operate at high temperatures and meet minimum strength requirements while remaining relatively lightweight.

Another important property of titanium and its alloys is corrosion resistance. Titanium will resist degradation in highly corrosive environments, such as sea water, making it a good candidate for offshore and naval applications. Additionally, titanium has a low impact on the human body and maintains a high biocompatibility. As a result, titanium and its alloys are a suitable material for use in medical tools and implants. Other unique properties of titanium are its low coefficient of thermal expansion, low thermal conductivity, and non-magnetic nature (Chandler, 1989; Air Force Materials Laboratory, 1972).

The improvements that are available for titanium alloys can be characterized by the general microstructural composition of a specific alloy. The microstructural distinctions between titanium alloys are defined into four

categories: α , β , metastable β , and α & β alloys. Depending on which alloying element is present in the material, different microstructures will dominate the titanium alloy (Figure 1.1). In turn, the final material properties exhibited by the alloy are dependent on which microstructure is present.

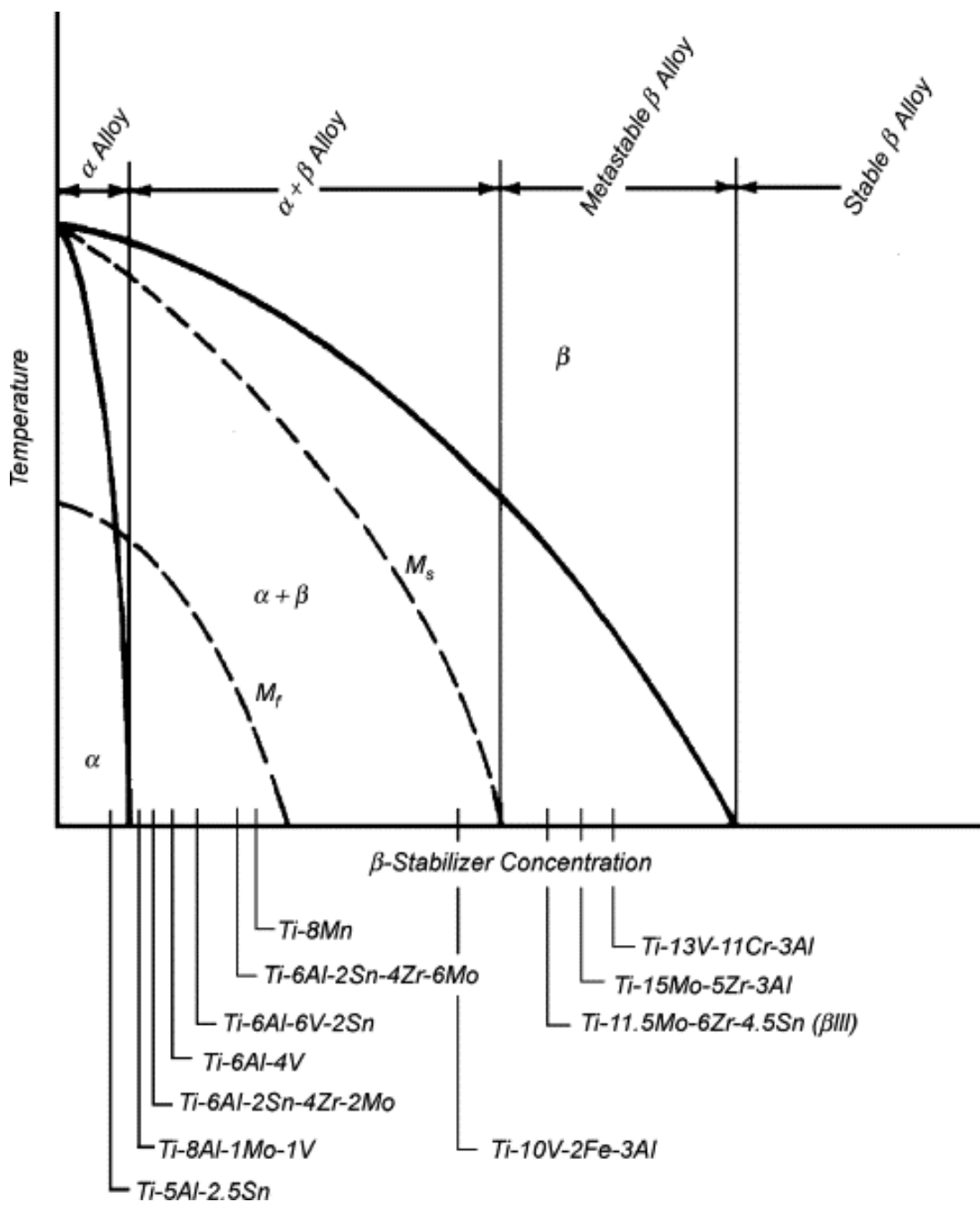


Figure 1.1: Generic isomorphous binary phase diagram of titanium (Zhecheva et al., 2005).

Among the many alloys of titanium, Ti-6Al-4V (Ti-64) dominates the market with 56% usage (Lutjering and Williams, 2003). For this study, two grades

of Ti-64 were used: grade 5, which meets AMS 4911 specifications, typically used in aerospace applications; and grade 23 (ELI or Extra Low Interstitial), which meets AMS 4931 specifications, typically used in medical applications. The chemical compositions of these materials are listed in Table 1.1 and Table 1.2. These alloys, when fully annealed, have the mechanical properties listed in Table 1.3 and Table 1.4.

Table 1.1: Ti-64 grade 5 workpiece with AMS 4911 specifications.

Element	Al	V	Fe	O	C	N	H	Y	Other - Total	Ti
Min	5.50	3.50	-	-	-	-	-	-	-	balance
Max	6.75	4.50	0.30	0.20	0.08	0.05	0.015	0.005	0.4	

Table 1.2: Ti-64 ELI grade 23 workpiece with AMS 4931 specifications.

Element	Al	V	Fe	O	C	N	H	Y	Other - Total	Ti
Min	5.50	3.50	-	-	-	-	-	-	-	balance
Max	6.50	4.50	0.25	0.13	0.08	0.03	0.0125	0.005	0.3	

Table 1.3: Ti-64 grade 5 mechanical properties for AMS 4911.

Density (kg/m³)	Ultimate Tensile Strength (MPa)	Yield Tensile Strength (MPa)	Modulus of Elasticity (GPa)	Poissons Ratio
4430	950	880	115	0.34

Table 1.4: Ti-64 ELI grade 23 mechanical properties for AMS 4931.

Density (kg/m³)	Ultimate Tensile Strength (MPa)	Yield Tensile Strength (MPa)	Modulus of Elasticity (GPa)	Poissons Ratio
4430	860	795	105	0.31

One of the main benefits of using Ti-64 is that it can be heat treated. This is a result of its ability to hold two microstructural phases, hexagonally close-packed (hcp, α) and body-centered cubic (bcc, β), at room temperature. In the fully annealed condition Ti-64 consists of mainly α phase, but the solubility of β increases with temperature. The β transus temperature for Ti-64 is 1100°C, when the microstructure completely transforms into β phase. In Ti-64, β phase is used to add strength, while α phase is primarily used for its corrosion resistance.

Temperature is also critical when identifying the strength of the material. All materials exhibit a loss in strength as temperature is increased, but titanium is known for its retention of strength at high temperatures; Ti-64 can maintain 80% of its ultimate tensile strength up to 600 °C (Figure 1.2). As a result, this alloy can be adopted for its strength in applications where a constantly elevated temperature is expected.

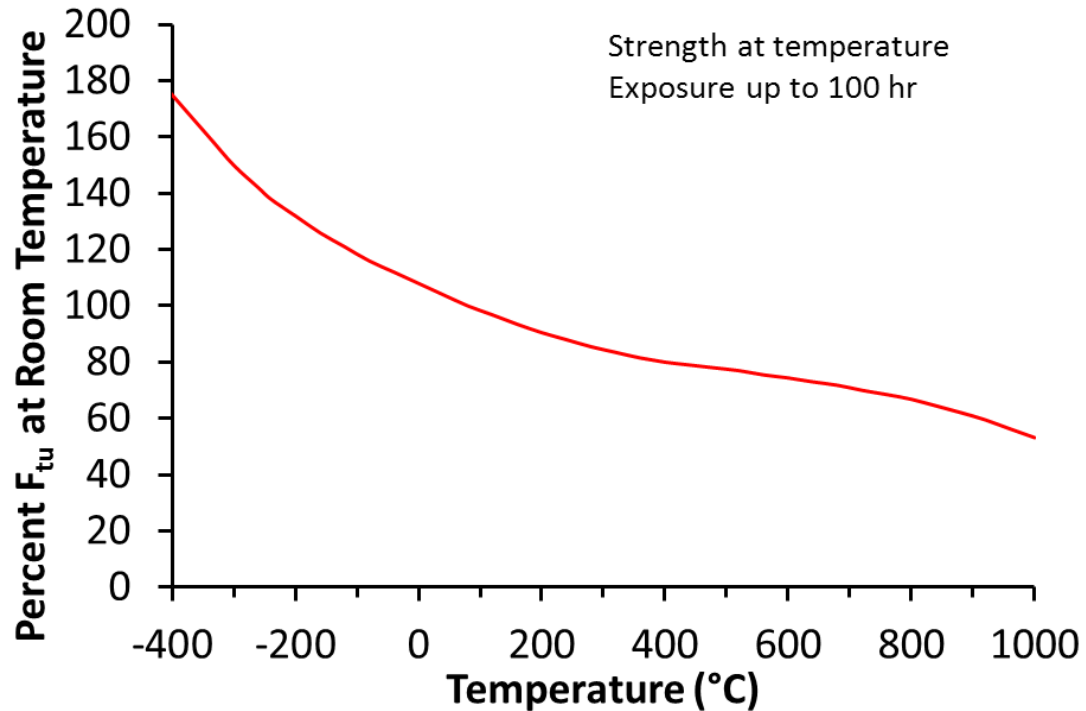


Figure 1.2: Percentage of ultimate tensile strength as a function of temperature for Ti-64 (Air Force Materials Laboratory, 1972).

Difficulties in machining Ti-64 are due in part to its retention of strength at high temperatures, its low thermal conductivity and high chemical affinity with tool materials. Because of this, Ti-64 is a good candidate for thermally-assisted machining. Since machining is a complex process, the unique material properties of Ti-64 are investigated in the current work.

1.3 Machining of Titanium Alloys

As previously noted, many of the advantages of advanced materials prove to be a problem when trying to alter the shape of a workpiece. The material's high strength at elevated temperatures causes higher forces to be required

during machining. Attendant low thermal conductivity of titanium alloys will typically result in high temperatures located very close to the tool cutting edge, which will result in rapid tool wear as the tool and workpiece are in contact with each other. As a result, the machining of titanium alloys can be costly and time-consuming due to limited speed that can be used and rapid wear of tools.

The poor machinability of Ti-64 is a direct result of its low thermal conductivity, strong chemical affinity with most tool materials, and the strong possibility of inhomogeneous deformation by catastrophic shear. The low thermal conductivity leads to very high temperatures on the tool face, which increases the wear rate of cutting tools. High temperatures also assist in chemical diffusion of titanium into the cutting tool material, which can lead to premature tool failure. The inhomogeneous deformation causes the cutting force to fluctuate and aggravates tool wear and chatter (Komanduri and von Turkovich, 1981; Chandler, 1989). As a result, Ti-64 is a difficult material to machine.

Of the different machining processes available, milling is critical to the manufacture of parts. Since the tool rotates and the workpiece remains stationary relative to the tool, milling has the ability to create very intricate parts. In the aerospace industry, almost all titanium monolithic components are manufactured by milling (Sun and Guo, 2008). Therefore, improvements in machinability for the milling process are critical for the present and future.

The characteristics of tool wear during titanium machining depend primarily on the speed of the cutting operation. When machining titanium at low speeds, tool wear is characterized by flank wear, which occurs on the tool

surface as it rubs along the workpiece, and crater wear, which occurs on the face of the tool. When machined at higher cutting speeds, premature chipping of the tool dominates tool wear. Due to the unpredictable nature of chipping and detrimental effect on machined parts, machining speeds have been limited to below 60 m/min in industry (Chandler, 1989).

However, higher speeds are desired in industry in order to produce parts more rapidly. As a result, many studies have investigated tool wear and failure mechanisms at higher cutting speeds using carbide and coated carbide tools. A brief summary of machining parameters are listed in Table 1.5. It was reported that all machining experiments employed down milling due to the increase in tool life that is achieved when cutting Ti-64. In addition, all testing applied a non-pressurized flood coolant during machining. The machining parameters presented in the table were used to establish experimental machining parameters for the work performed in this thesis.

Table 1.5: Machining parameters for Ti-64.

Literature	Cutting Speed (m/min)	Depth of Cut (mm)	Width of Cut (mm)	Feed per Tooth (mm/tooth)	Tool Diameter (mm)	Tool Material	# of Flutes/ Inserts
Wan et al. (2011)	24-30	0.4-0.5	2-2.5	0.03-0.08	12	Carbide	4-flute
Kuljanic et al. (1998)	90-160	0.3	5	0.125	-	PCD	-
Jawaid et al. (2000)	55-100	2	58	0.1-0.15	80	Coated Carbide	6-insert
Sun and Guo (2008)	50-110	1.5	4	0.06-0.14	12.7	Coated Carbide	4-flute
Rao (2006)	121.9	0.762	3	0.0508	101.6	Carbide	1-insert
Sun and Guo (2009)	50-110	1.5	2-6	0.06-0.14	12.7	Carbide	4-flute
Thomas et al. (2010)	200	5	1	0.05	16	Carbide	4-flute
Amin et al. (2007)	40-160 120-250	1 1	32 32	0.1 0.1	32 32	Carbide PCD	2-insert 2-insert

No significant improvement in cutting speed has been found for machining Ti-64 using uncoated carbide tools. Additionally, those tests could not eliminate premature chipping that limits cutting speed during Ti-64 machining. Early comparisons between HSS and steel coated tools indicated that coatings can provide an increase in tool life. An overall improvement of 8% in tool life was found when using TiCN coated tools instead of standard HSS tools (Lopez de Lacalle et al., 2000). A comparison of uncoated carbide tools with W–Ti/Ta/Nb and TiC+Ti/CN+TiN coated carbide tools indicated that a comparable tool life for the different tools could be achieved when machining Ti-6242S alpha-beta titanium alloy (Che Haron et al., 2007).

Studies into machining with polycrystalline diamond (PCD) cutting tools were also performed. From the results of this testing, tool life was shown to increase (Kuljanic et al., 1998); however, the costs associated with these tools tend to limit their application in industry. Recent studies have shown the potential for increased cutting speeds using PCD tools (Amin et al., 2007), but an economic analysis has not been performed.

Tool wear occurs through the several interactions between the cutting tool and workpiece, and therefore factors other than tool material can influence final machinability of Ti-64. Among the most critical factors during milling are cutting tool pressure and friction. Many studies have investigated how alternative methods of applying a coolant would influence tool wear by reducing tool pressure and friction during milling.

One approach (Lindeke et al., 1991; Kovacevic et al. 1995) used a coolant under high pressure, directed at the cutting tool, to assist in material removal. Although some improvement in tool life was found, these studies did not investigate whether machining speed could be improved using this technique. Another approach used a lower-temperature coolant on the cutting tool during machining (Hong et al., 2001; Su et al., 2006). By using compressed cold nitrogen to cool the tool face and flank, longer tool life and higher cutting speeds were achieved. The study in this thesis has incorporated the results reported in previous works to choose tool materials and machining speeds to characterize the machinability of titanium alloys by current practice.

1.4 Literature Review of Laser-Assisted Machining

Thermally-assisted machining has been studied for many years. Early work with this approach utilized propane torches, oxyacetylene torches, and induction coils as a heating source, each resulting in varying degrees of success. The main challenge encountered by these attempts was the difficulty in controlling the application of heat and ensuring that only the workpiece to be removed was affected (Pfefferkorn et al., 2009).

1.4.1 Laser-Assisted Turning

In the late 1970's, lasers were developed that could overcome the challenges of controlling the heat application. These lasers were capable of

producing intense heat in a precise area, which allowed for the study of laser-assisted machining (LAM) of difficult-to-machine materials.

Konig and Zaboklicki (1993), Rozzi et al. (1997, 1998, 2000), and Lei et al. (2001) showed that LAM could be applied to ceramic workpieces to perform turning operations, whereas previously only grinding processes were possible. The use of LAM on these workpieces achieved a much higher material removal rate and improved surface finish. Rozzi et al. (1998; 2000) performed temperature prediction through numerical modeling methods within the workpiece during LAM. Anderson et al. (2006) showed that LAM can be performed economically on difficult-to-machine materials, as a result of the advances achieved in the laser technology and reduction in equipment cost.

Dandekar et al. (2010) investigated LAM and hybrid machining techniques for a Ti-64 alloy. The work included thermal modeling for temperature prediction to determine a parametric equation of temperature with respect to machining and laser parameters. Cutting force prediction was performed using AdvantEdge and the Johnson–Cook model, and a close agreement was found between predicted forces and experimental results. The study showed that cutting force was reduced with laser power and the cutting force could be reduced by 33% using LAM. The hybrid machining technique of using laser heating of the workpiece and cryogenic cooling of the cutting tool could improve tool life by two fold up to speeds of 150 m/min, while LAM alone produced an improvement in tool life of 1.7 times for speeds below 100 m/min. Microstructural comparison showed no

difference between the LAM process and traditional machining at equivalent machining speeds.

Rahman Rashid et al. (2012) studied LAM of Ti–10V–2Fe–3Al, a beta titanium alloy. It was determined that for slow cutting speeds, cutting force could be reduced by LAM to a half of the amount measured during conventional machining. However, as machining speed was increased, the reduction in cutting force was reduced, and there was no significant cutting force reduction beyond cutting speeds of 175 m/min. Their study also showed that both LAM and traditional machining resulted in a change from continuous chips to segmented saw-tooth chips at speeds close to 50 m/min.

1.4.2 Laser-Assisted Milling

The turning process is limited to producing axisymmetric part shapes. On the other hand, milling can produce many complex parts with arbitrary geometry. The differences between turning and milling give rise to potential challenges to laser assisted milling, which require further investigation. Studies have been performed to determine if laser-assisted milling (LAML) can improve machinability while accounting for the differences between continuous chip formation during turning and the interrupted nature of chip formation during milling.

Recent studies (Shelton, et al. 2010a; 2010b) carried out laser-assisted micro-milling on the difficult-to-machine materials of AISI 316, AISI 422, Ti-64 and Inconel 718 by using side milling and slotting configurations. Improvements

were found in surface finish on the final workpiece, along with a reduction of edge burrs and a reduction in cutting force as indicated by numerical modeling AE sensor readings. This study showed the feasibility and general improvement that LAML could provide when machining these materials.

Wiedenmann et al. (2011; 2012) presented temperature prediction work and experimental testing using a laser-assisted face milling setup. Modeling work was used to predict temperatures within the workpiece during the LAML process for a Ti-64 alloy. Modeling included a regression analysis of cutting force in terms of several machining factors such as feed, laser power, and laser lead. Regression analysis showed that the best results in cutting force reduction could be achieved by the use of higher laser power and smaller laser lead distance. A numerical database for predicting a heat-affected zone was created based on the modeling work and experimentally validated using optical inspection of machined workpiece cross-sections.

Sun et al. (2011) presented experimental work on LAML of a Ti-64 alloy using up-milling. Basic temperature prediction was performed to determine the temperature of the workpiece at a point on the top surface, and the depth of cut, during the laser heating process. They showed that as laser power was increased, the cutting force in the feed direction decreased. Tool life comparisons by the machining tests showed that LAML produced less wear than traditional milling, but that high laser power would result in melting of the workpiece surface, which would produce chipping of the insert as the tool interacted with this material.

Brecher et al. (2010) integrated a laser into a milling machine spindle and performed LAML experiments on an Inconel 718 workpiece. Through coordination of laser heating during tool rotation and workpiece interaction cutting force was reduced. After machining was performed over a set amount of time, using both LAML and traditional methods, a comparison of flank wear showed that overall tool life was improved with the use of LAML.

Ding et al. (2012) performed a detailed analysis of the thermal and mechanical processes that occur during laser-assisted micro-milling of 422 SS, Inconel 718, and Ti-64 in a side milling configuration. Modeling was performed to predict cutting forces during machining where a good agreement was found with experimental results. It was determined that LAML successfully reduced the tool wear rate from 0.73 to 0.12 $\mu\text{m}/\text{min}$ for 422SS fin side cutting.

1.5 Objectives

The main objective of this study is to examine the milling of two Ti-64 alloys in order to quantify the improvement possible through the use of LAML. To achieve this goal, the following tasks are carried out:

- 1) Thermal modeling is performed to characterize the temperature profile within the workpiece
- 2) Tool wear, cutting force and surface properties will be experimentally determined
- 3) To avoid any detrimental alteration of the final workpiece material properties as a result of laser heating, a detailed study of final workpiece

microstructure will be performed to identify if this goal has been achieved for the LAML settings chosen

- 4) An economic analysis is carried out for comparison between traditional milling and LAML
- 5) Investigation into the feasibility of LAML to produce unique shapes will be performed. Due to the complexity inherent in milling, a system will be created to integrate laser control with a 4th machining axis to allow for milling of complex contours.

CHAPTER 2. EXPERIMENTAL SETUP AND THERMAL MODELING

2.1 Experimental Setup

Milling experiments were performed on a MAZAK VQC-40/15 vertical milling center with a MAZATROL- M32 controller. The machine has a maximum spindle speed of 6000 RPM and maximum power of 7.5 HP. An IPG Photonics Ytterbium laser system (YLS-1000) was used, which produced a 1071 nm wavelength laser and had a maximum power output of 1000 W. A laser delivery system was designed and integrated with the MAZAK milling center to direct the laser beam onto a workpiece surface at a specified distance ahead of the cutting tool. Physical constraints of the milling machine and fiber-optic cable were taken into account to create a custom laser head. The resulting laser delivery system consisted of a collimating lens, a focusing lens and two mirrors that reflected the beam 90 ° to irradiate the surface of the part. It also allowed for two degrees of freedom in motion via a telescoping tube and a rotational axis so that the focused laser beam could be positioned in a desired location. This delivery system was mounted onto the MAZAK milling machine using a custom fixture.

The final laser spot size was calculated and measured to be 2.5 mm x 3.6 mm in an elliptical shape with a Gaussian power distribution. Laser spot length was calculated from the total distance from the focusing lens to the surface of the workpiece ahead of the cutting tool, and was based on beam parameters and focusing lens properties. The laser beam width was determined from the 41° angle of incidence (from the horizontal) of the laser beam onto the surface of the part. To minimize excess heat flowing into the workpiece, the width of cut was kept roughly the same as the laser spot width. Due to the Gaussian distribution of the laser energy, the majority of the experiments were performed using a 3.0 mm radial width of cut. To keep the laser head safe in the workspace and to keep the laser from being reflected into the tool, machining was performed in the Y-axis direction of the MAZAK machine. A general overview of the laser delivery system and its influence on the laser spot position can be seen in Figure 2.1. The beam position with respect to the cutting tool is schematically shown in Figure 2.2.

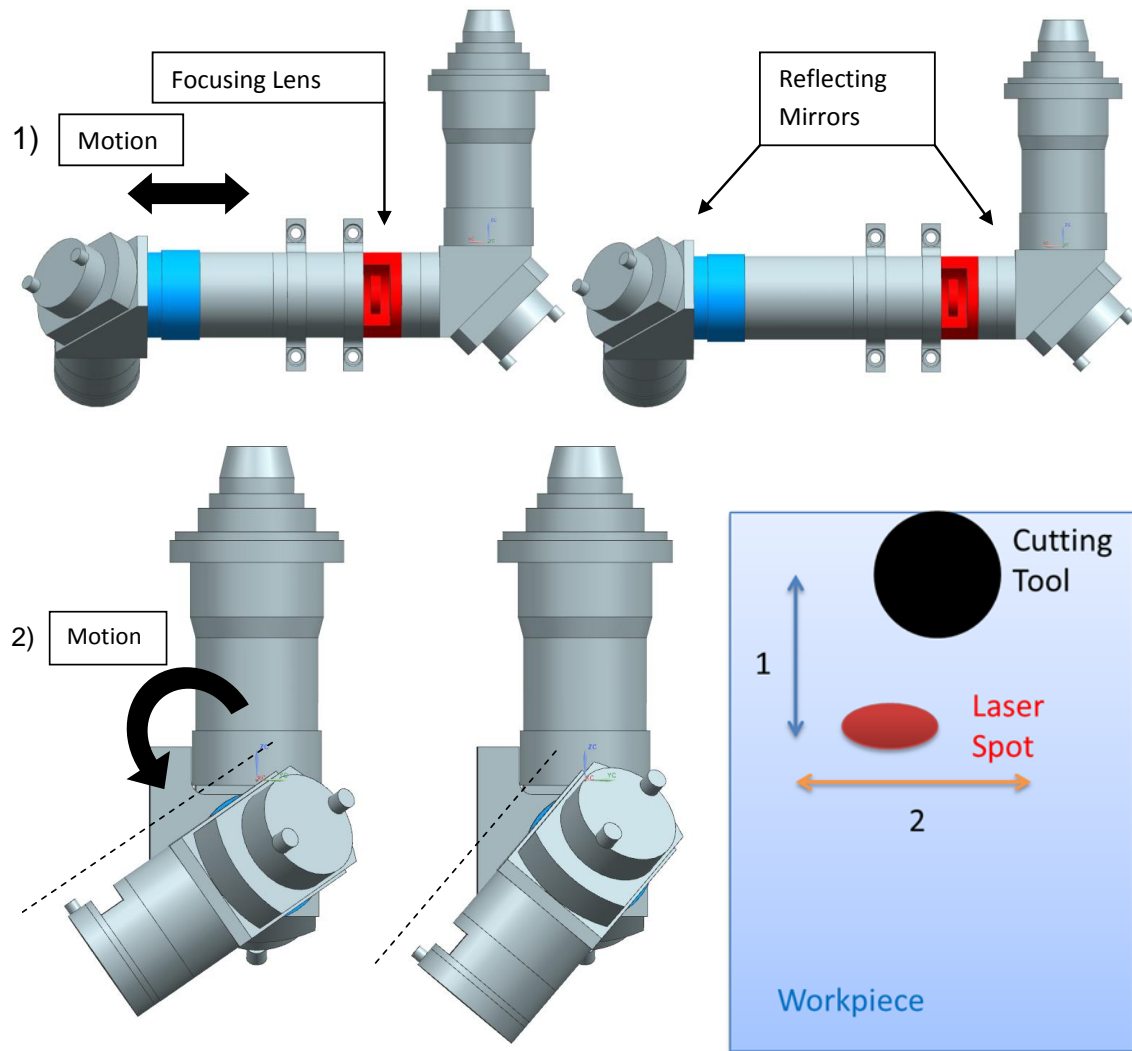


Figure 2.1: Laser head degrees of freedom and laser spot setup.

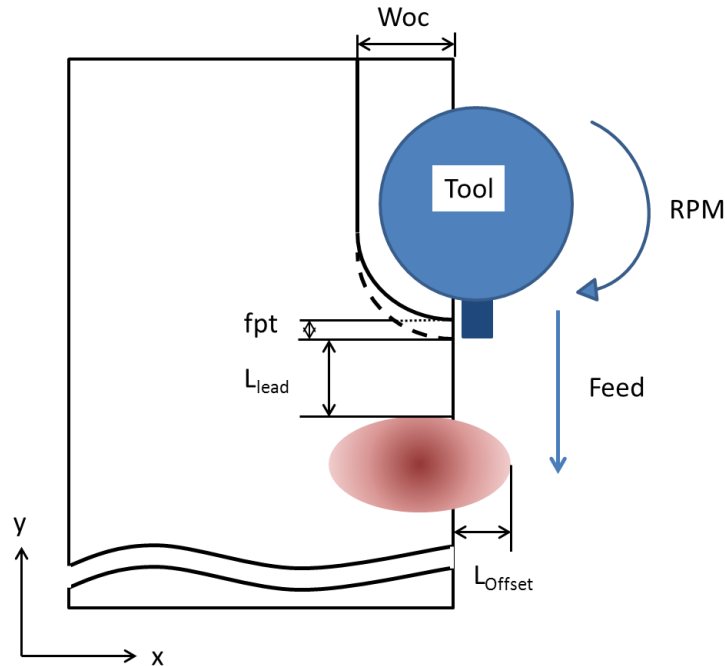


Figure 2.2: General machining setup for LAML (top view).

A Kennametal Mill 1-14 tool holder with KC520 and KC725M carbide grade inserts were used for Ti-64 machining tests. The specific parameters of the cutting tool and inserts are listed in Table 2.1. Single insert cutting was used during all tool wear and force testing. Down milling was used in all titanium machining experiments due to the reported decrease of tool life when upmilling is employed.

Table 2.1: Cutting tool parameters.

Kennametal Tool Holder	Kennametal Insert	Insert Type
M1D075E1402W075L175	EDPT140408PDERHD	KC520 Coated Carbide
M1D075E1402W075L175	EDPT140408PDSRGD2	KC725M TiAlN PVD Coated Carbide

Tool Diameter	Lead angle	Radial rake	Axial rake	Nose radius
19.05 mm	0°	15°	3°	0.8 mm

A flood coolant was applied during traditional machining experiments, which consisted of a mixture of 5% oil and water. Argon gas was used as an assist gas during LAML to keep the chips from blowing into the laser delivery optics and reduce the possibility of fire within the experimental setup. The argon gas was applied using two jets, one coming out of the laser head and the other aimed at the rear of the cutting tool with 0.35 MPa in pressure and 0.47 lpm in flow rate for both. Workpiece size for Ti-64 grade 5 was 50x100x190 mm³ and 50x60x90 mm³ for tool wear and force experiments, respectively. The workpiece size for Ti-64 ELI grade 23 was 150x125x50 mm³ for both tool wear and force experiments.

K-type thermocouples were attached to the sample and LabVIEW software was used to record temperature measurements at a rate of 10 kHz during heating tests with the laser. The surface temperature was also recorded using a FLIR ThermoCAM SC 3000 infrared camera (IR camera) with a detection

wavelength of 8,500 nm. Images were captured at 50 Hz and recorded based on the workpiece emissivity. Details of the IR camera characteristics as provided by the manufacturer are listed in Table 2.2.

Table 2.2: IR camera characteristics.

FLIR SC3000 Infrared Camera	
Detector type	GaAs, Quantum well infrared photon (QWIP)
Wavelength (nm)	8000-9000
Temperature Range (°C)	-20 to 1500
Maximum Sample Frequency (Hz)	60
Sensitivity	0.03°C at 30°C
Accuracy	±2% or 2°C

A Kistler 3 component dynamometer type 9257B with a Kistler 5004 dual mode amplifier was used to measure force data with LabVIEW software at a sampling rate of 2 kHz for Ti-64 cutting force experiments. Tool wear measurements were taken using a Nikon Eclipse LV150 optical microscope and recorded using a SPOT Insight Firewire camera and software.

A Mitutoyo hardness tester (model ATK F1000) was used to determine the surface hardness in the HRC scale using 150 kgf load and a 120° diamond cone indenter. All measurements were taken on the final workpiece surface.

Microhardness analysis was performed using a LECO KM 247AT machine.

Hardness was recorded using a Vickers hardness scale using a 200 g load and a dwell time of 13 seconds. Indentation size was measured and used to determine final hardness of the samples. Measurements were taken at specific depths

below the machined surface to determine the change in hardness with respect to distance. Hardness at a very shallow depth could not be measured accurately as the workpiece would deform when the indenter was too close to the edge.

A Bruker D8 Focus X-Ray Diffractometer was used for XRD analysis of Ti-64 samples, which has a Cu-K(α) source, a 3 circle goniometer, and a Lynseye 1D detector. A scan step of 0.024° was used with a counting time of $8^\circ/\text{min}$. Residual stresses were measured on the Ti-64 samples using the X-ray diffraction technique on Bruker D8 Discover X-Ray Diffractometer with General Area Detector Diffraction System (GADDS) using Cr-K(α) radiation ($\lambda=0.22897\text{nm}$) at 30kV, 50mA to acquire {103} diffraction peaks at 2θ angles of about 119.3° using a spot of 0.8mm collimated from the 2 mm beam. A two-dimensional approach was used to evaluate the 2D diffraction data. The detector was set at $D=16.77\text{cm}$ and the ψ -tilt was achieved by ω rotation. Residual stress data was collected from $\psi=0^\circ$ to 30° with 10° steps. The data processing and stress evaluation were performed with GADDS software and Materials Data Incorporated's Jade, respectively. Young's modulus of $E=110\text{GPa}$ and Poisson's ratio $\nu=0.36$ were used to calculate the residual stress. For peak fitting a pseudo-Voigt function was used. Depth profiles for the residual stresses were measured by chemically etching successive layers of the material by electropolishing using an etchant of 8% HF and 92% H_2O , with an etching interval of 40 sec to remove $25\ \mu\text{m}$ of material.

2.2 Ti-64 Thermal Modeling and Validation

A prismatic thermal model based on transient conduction was developed for laser heating and material removal earlier by Tian et al. (2006). Thermal history from the thermal model was used to predict the resulting temperature within the Ti-64 workpiece as it underwent laser-assisted machining. Predicted temperatures were used to optimize laser parameters and ensure that final workpiece properties after machining would not be significantly influenced.

The primary heat transfer effects that influence the laser heating and material removal of a prismatic part of Ti-64 are as follows:

- laser beam irradiation on the metal surface and penetration of the absorbed heat flux,
- convective heat transfer from the heated spot to the assist gas jet,
- radiation heat transfer from the heated surface to the surroundings,
- convective and radiation heat transfer from the non-heated surfaces to the surroundings,
- conduction of the heat away from the heated surface into the bulk material, and
- elimination of material over time

The thermal model for laser heating and material removal of prismatic parts incorporates all of these effects when making temperature predictions.

Temperature-dependent thermophysical property data for thermal conductivity and specific heat were incorporated into the model to provide accurate results.

2.2.1 Mathematical Formulae and Assumptions

The setup for laser-assisted milling was based on a stationary workpiece and a translating laser heat source and cutting tool as shown in Figure 2.3. The setup consisted of a laser traveling along the X direction at a given Y location. The numerical model for laser-assisted machining developed by Tian et al. (2006) has the following features:

- It uses an implicit finite difference method for transient conduction.
- Laser spot can be defined as Gaussian, top hat, or user-defined for elliptical, circular or rectangular beam geometry.
- Isotropic thermal conductivity is used.
- It defines assist gas functionality and how it travels with the laser beam.

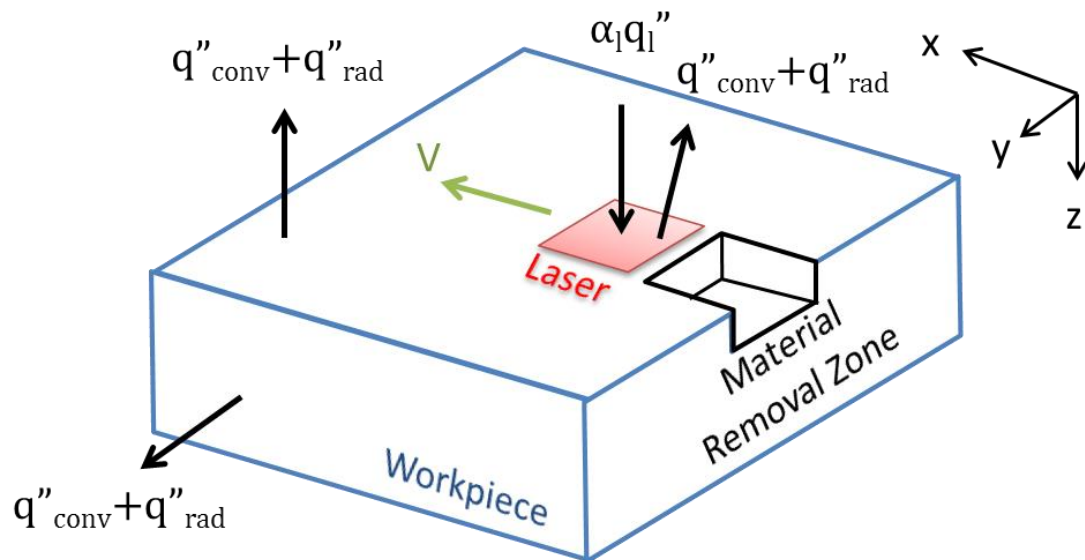


Figure 2.3: Prismatic thermal model boundary conditions.

The prismatic thermal model for laser heating and material removal is based on the energy diffusion equation for three-dimensional transient conduction:

$$\frac{\partial h(T)}{\partial t} = \frac{\partial}{\partial x} \left(k(T) \frac{\partial T}{\partial x} \right) + \frac{\partial}{\partial y} \left(k(T) \frac{\partial T}{\partial y} \right) + \frac{\partial}{\partial z} \left(k(T) \frac{\partial T}{\partial z} \right). \quad (2.1)$$

Thermal properties for the workpiece material, such as specific heat and thermal conductivity, are temperature-dependent and assumed to be isotropic. The density of the material is considered to be constant and uniform.

The top surface of the workpiece for laser heating and air jet interaction is described by

$$k \frac{\partial T}{\partial z} \Big|_{z=z_0} = \alpha_l q_l''(x, y) - q_{conv}'' - q_{rad}''. \quad (2.2)$$

where k is the thermal conductivity (W/m-K), α_l is the absorptivity of the workpiece surface to irradiation from the laser, q'' is the heat flux (W/m²), and T is temperature (K). The distribution of laser energy $q_l''(x, y)$ on the workpiece is determined by the actual beam profile supplied by the laser manufacturer. Free convection is used to determine the heat flux from convection, q_{conv}'' . The radiation from the material to its surroundings, q_{rad}'' , was determined using ambient temperature, workpiece temperature and total emissivity of the Ti-64 workpiece. This was estimated as 0.2 in the temperature range of 25 °C to 1200 °C. For the top surface not impacted by the laser beam, the laser irradiation term is dropped:

$$k \frac{\partial T}{\partial z} \Big|_{z=z_0} = -q''_{conv} - q''_{rad} . \quad (2.3)$$

Boundary conditions for the bottom of the workpiece are assumed to be adiabatic, and thus heat transfer for the bottom surface is assumed to be zero.

$$k \frac{\partial T}{\partial z} \Big|_{z=z_D} = 0 . \quad (2.4)$$

Boundary conditions for the sides of the workpiece use free convection and radiation with the surroundings, with the temperature set as the ambient temperature of the room:

$$k \frac{\partial T}{\partial z} \Big|_{\substack{x=0 \\ x=x_L}} = -q''_{conv} - q''_{rad} , \quad (2.5)$$

$$k \frac{\partial T}{\partial z} \Big|_{\substack{y=0 \\ y=y_W}} = -q''_{conv} - q''_{rad} . \quad (2.6)$$

Initial temperature of the workpiece is assumed to be the same temperature as that of the surroundings:

$$T(x, y, z, t = 0) = T_{sur} . \quad (2.7)$$

To simulate material removal, position of the tool is set relative to the laser irradiation. Control volumes have their conduction, convection and radiation set equal to zero in the areas of material removal. Subsequent calculations for active control volumes do not use the data from these 'removed' control volumes when calculating the temperature of the workpiece.

2.2.2 Temperature Dependent Properties

In order to model temperatures within the workpiece, accurate material properties must be known. For the most accurate results, temperature-dependent properties should be used. The temperature-dependent properties needed for the prismatic thermal model include specific heat and thermal conductivity. Equations for Ti-64 properties were obtained from literature data (Touloukian, 1970) and are shown in Figure 2.4. It was found that as a result of the small chemical differences between grade 5 and grade 23, there is not a significant difference in thermal properties for these Ti-64 alloys. Therefore, modeling was performed for both materials using the data obtained from literature.

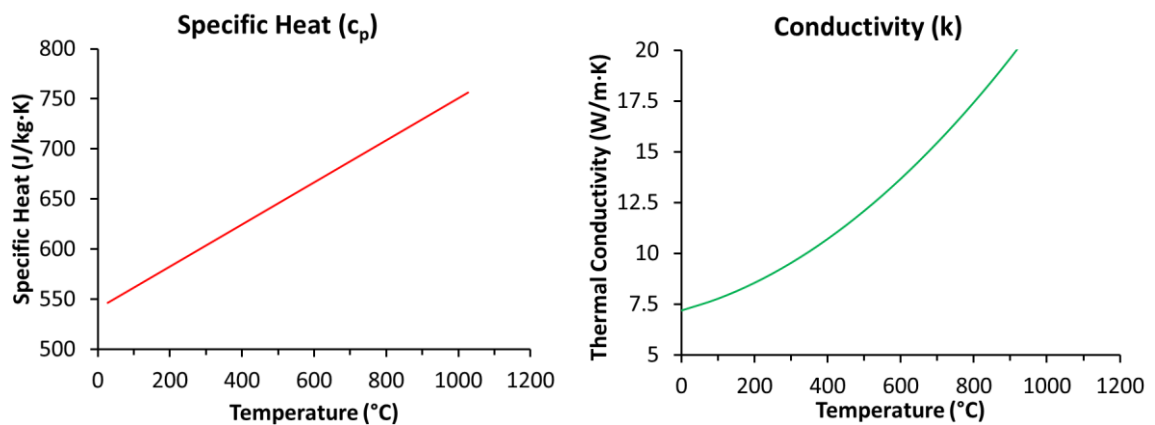


Figure 2.4: Specific heat and thermal conductivity of Ti-64 (Touloukian, 1970).

Based on the temperature-dependent data, specific heat was approximated using a linear relationship and thermal conductivity was approximated using a second-order polynomial. These equations are presented in Table 2.3.

Table 2.3: Temperature dependent property equations for Ti-64.

Thermal Conductivity, k (W/m K)	$= 6.65 - 0.0012 * T (K) + 1 * 10^{-5} * T^2 (K)$
Specific Heat, c_p (J/kg K)	$= 415.52 + 0.2293 * T (K)$

2.2.3 Laser Absorptivity

Emissivity of the workpiece and material absorptivity of the laser are among the material properties that are critical to predicting LAML temperatures through thermal modeling. Since the laser energy that enters the material is approximated using a surface heat flux, an accurate value of laser absorptivity by the workpiece is of critical importance. Material absorptivity is dependent on the wavelength of the laser irradiating the workpiece, the composition and surface condition of the workpiece material and temperature. A review of the literature resulted in obtaining optical properties for the emissivity (ϵ) and absorptivity (α_n) for a Ti-64 alloy to an Nd:Yag laser (Yang et al., 2010). Since the Nd:Yag laser wavelength (of 1064 nm) is very close to that of a fiber laser (1071 nm), a similar value to 0.35 is expected for fiber laser absorptivity (α_f) for a Ti-64 workpiece, but must be verified experimentally.

Heating experiments were performed using a fiber laser directed onto the surface of a Ti-64 workpiece. A laser scan speed was used, which would simulate conditions similar to those during actual cutting experiments. A target cutting speed of 46 m/min was set based on the parameters: feed per tooth (f) of 0.1 mm/tooth, spindle rotation (N) of 764 RPM, and tool diameter (d) of 19.05 mm. From this, a laser scan speed of 76.2 mm/min was used to simulate an

equivalent cutting speed of 46 m/min in the Ti-64 laser heating tests. Images were recorded with an infrared thermal imaging camera (FLIR ThermoCAM SC 3000).

In order to get accurate temperature readings, it was necessary to determine emissivity data for the workpiece to the IR camera wavelength by using previous experimental work with Ti-64 (Hahn et al., 2006). From the literature, laser heating was performed with temperatures recorded by the IR camera, and thermal modeling was performed for the Ti-64 workpiece based on the known absorptivity data. Emissivity values were determined based on the thermal model results and IR camera readings as shown in Figure 2.5, where it was found that surface emissivity values increased as the temperature increased.

For the work in this thesis, the emissivity values from literature were used in the IR camera software to accurately interpret the temperature of the Ti-64 workpiece during heating experiments using a fiber laser. IR camera settings for the device and external protective optics are listed in Table 2.4 and an image recorded during IR camera experiments is shown in Figure 2.6.

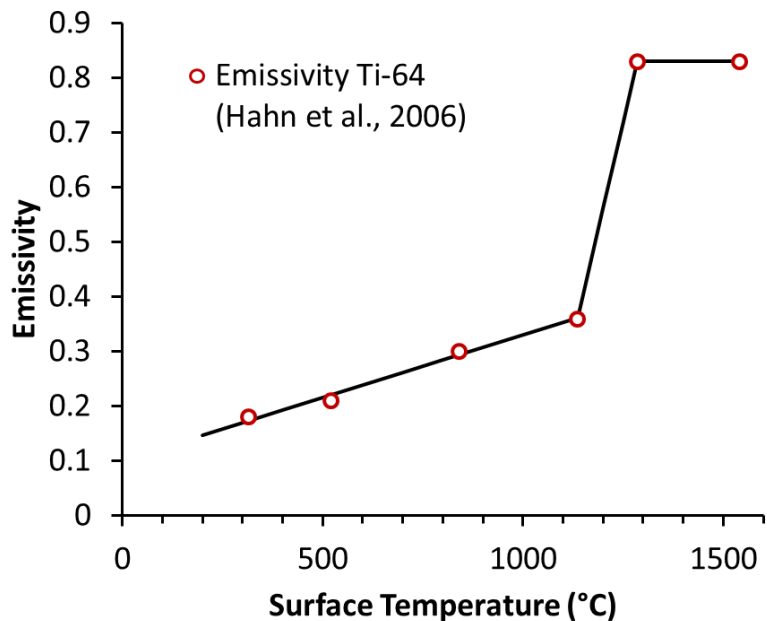


Figure 2.5: Plot of emissivity vs. Ti-64 surface temperature at 8500 nm wavelength for IR Camera from literature (Hahn et al., 2006).

Table 2.4: IR camera settings.

		External Optics		Environmental Settings	
Distance to Object	Ambient Temp (°C)	Transmissivity	Ambient Temp (°C)	Relative Humidity	Ambient Temp (°C)
0.5 m	23	0.93	23	50%	23

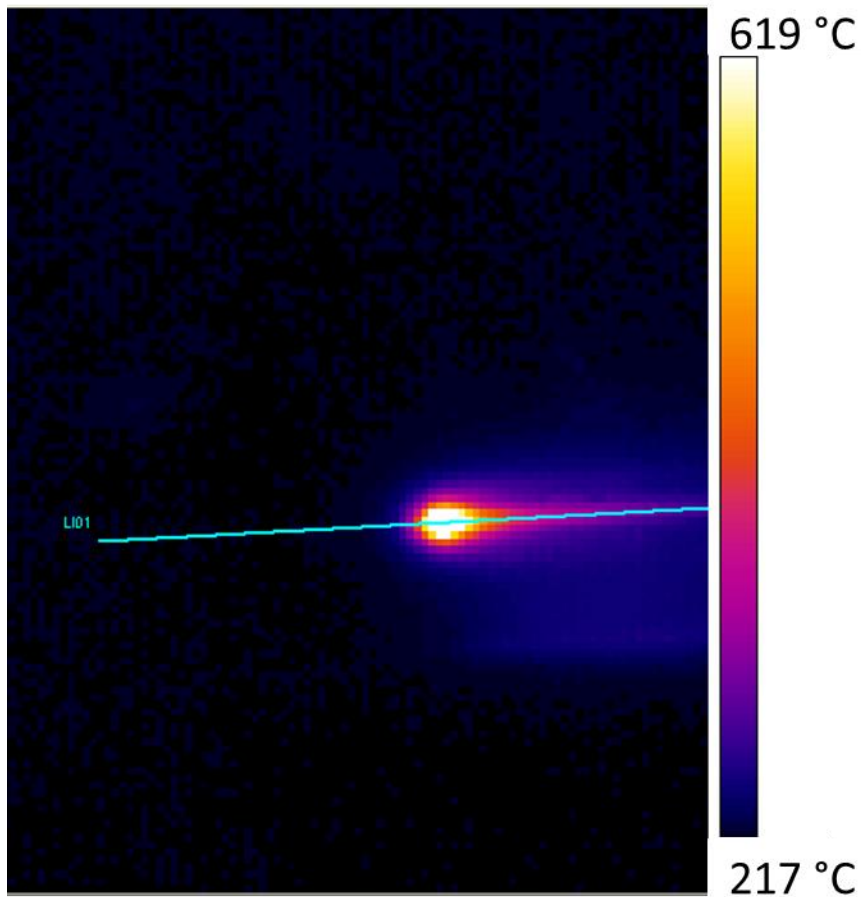


Figure 2.6: IR camera image of workpiece surface during laser heating.

Heating experiments were performed using the fiber laser to irradiate a Ti-64 workpiece with temperature measurements recorded by the IR camera at a rate of 50 Hz. Temperature measurements were analyzed using the thermal camera software. Temperatures were determined by creating a line along the length of the laser scan and then recording the maximum temperature of the workpiece along the line.

The prismatic thermal model was used to determine temperatures within the workpiece based on the material properties of Ti-64, as well as the cutting

conditions used in the heating experiments. Simulations duplicated the conditions of the experiments, while the laser absorptivity of the workpiece was varied. By comparing the simulated temperature of the workpiece surface to the temperature recorded by the IR camera, accurate absorptivity values could be determined for the four different laser power levels used during experiments (Figure 2.7).

It was found that oxidation of the surface became apparent for laser power levels above 100 W (Table 2.5) or a surface temperature of 1100 °C. This was not discussed in the literature, and may not have occurred during the laser heating experiments due to the presence of excessive argon flooding. High volume flooding on the workpiece surface is not typical during LAML and not implemented during the absorptivity testing performed in this study.

A change in laser absorptivity is appropriate when laser power is high enough to produce an oxide layer on the workpiece surface. From the experiments and modeling work, laser absorptivity of 0.35 was obtained for low laser power with no oxidation present, while laser absorptivity of 0.5 was determined for higher laser power that resulted in an oxide layer. A summary of the experiments performed and images of the final surface are shown in Table 2.5.

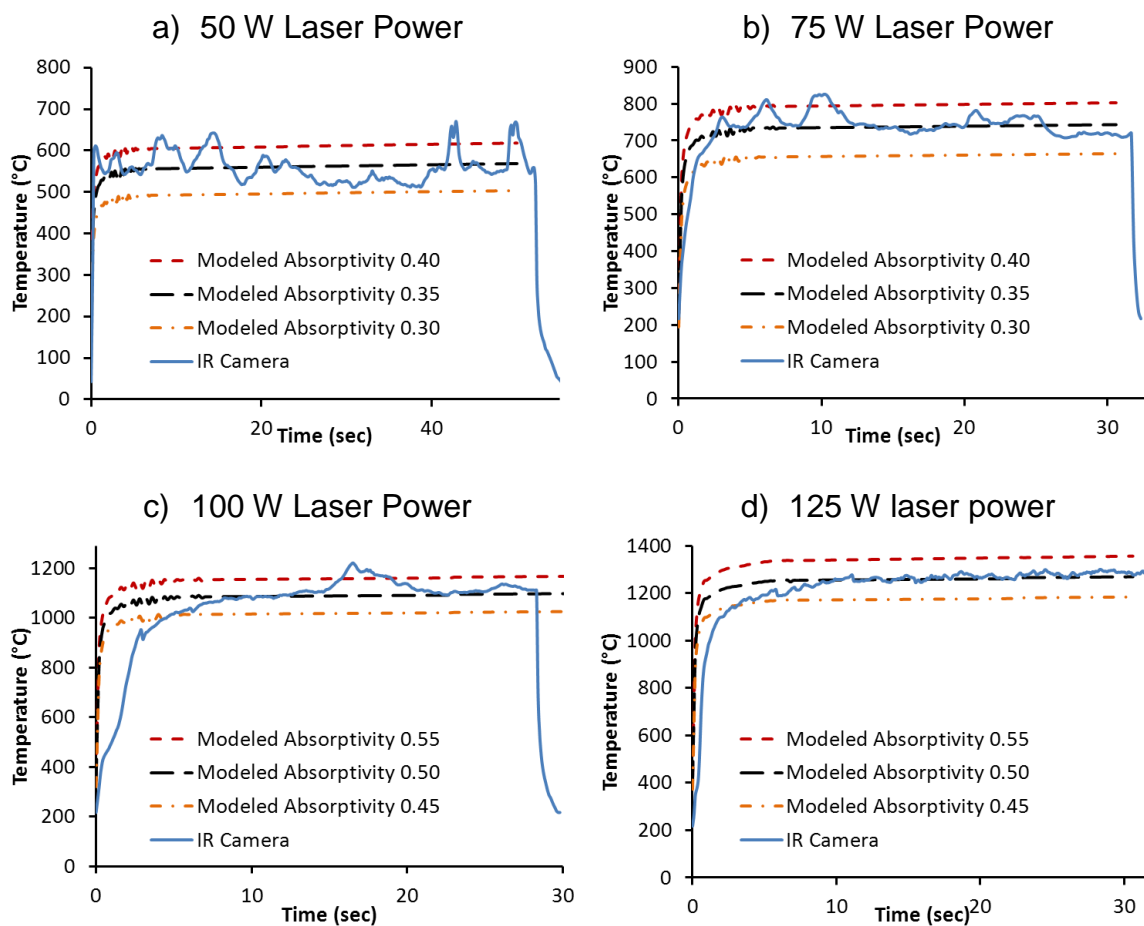






Figure 2.7: IR camera temperature results and thermal model temperature prediction for maximum workpiece temperature.

Table 2.5: Heating test conditions and results.

Test	Power (W)	T _{max} (°C)	ϵ	α_f	Sample Surface
HT1	50	560	0.22	0.35	 560 °C
HT2	75	740	0.27	0.35	 740 °C
HT3	100	1150	0.5	0.5	 1150 °C
HT4	125	1250	0.73	0.5	 1250 °C

Based on the results of the IR camera and thermal modeling work, laser absorptivity values of 0.35 and 0.5 were used for Ti-64 modeling work, with changes depending on the formation of an oxide layer during heating. It was found that this oxide layer would develop when the surface temperature exceeded 1100°C. As a result, this temperature was used as the threshold value for changing workpiece absorptivity during modeling. It was also observed that as the laser power increases, the width of the oxidation can also increase, as seen in Table 2.5. Such an increase in oxide width can affect the required machining parameters, such as width of cut.

Validation of the calculated absorptivity values was performed for a Ti-64 grade 5 workpiece. Modeling was performed for laser power levels of 115 W, and 130 W. With the surface temperature results based on a 0.5 absorptivity value, laser heating experiments were performed using the IR camera. A good agreement was found between the modeled temperature prediction using the

calculated absorptivity value and the measured temperature of the workpiece surface as shown in Figure 2.8.

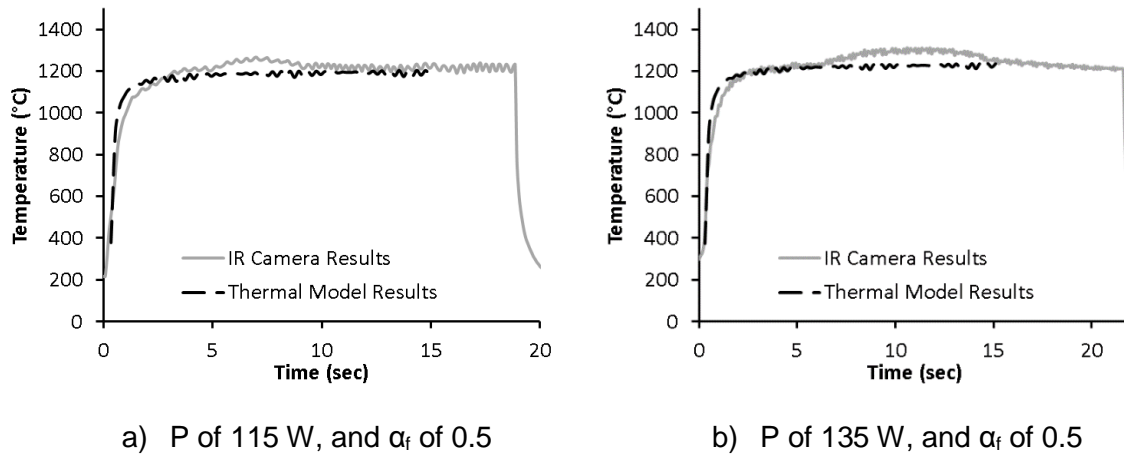


Figure 2.8: Absorptivity validation for Ti-64 grade 5.

2.2.4 Statistical Modeling for Temperature Prediction

The prismatic thermal model was used to determine the average temperature within the cutting zone (T_{mr-ave}) for the workpiece using parameters for the laser as shown in Table 2.6, experimental cutting conditions, and Ti-64 workpiece properties. Simulations were run using a full factorial design to change parameters of feed rate and laser power and all conditions according to Table 2.7.

Table 2.6: Constants used in thermal model.

Laser Spot size (mm)	Woc (mm)	L _{lead} (mm)	α_f	ϵ	ρ (kg/m ³)	Simulated Length (mm)
2.5 x 3.6	3	3.5	$\alpha_f = 0.35$ $T_{\max} < 1100^\circ\text{C}$ $\alpha_f = 0.5$ $T_{\max} > 1100^\circ\text{C}$	0.21	4430	20.8

Based on laser absorptivity testing for a fiber laser, temperature distributions were modeled using two values of absorptivity on the Ti-64 surface, and an example of the temperature output is shown in Figure 2.9. Due to the presence of an oxide layer, the final surface temperature on the Ti-64 workpiece was used to determine if oxidation would be present and the appropriate laser absorptivity was used in the model. Temperature predictions were used to determine the maximum temperature of the workpiece (T_{\max}), the average temperature in the cutting zone ($T_{\text{mr-ave}}$), and the maximum temperature at the final depth of cut (T_{machined}).

Table 2.7: Thermal model conditions.

V	f	F	Power	α_f
m/min	mm/tooth	mm/min	W	
37	0.1	61.82	100	0.35
37	0.1	61.82	125	0.5
37	0.1	61.82	150	0.5
37	0.1	61.82	175	0.5
50	0.1	83.55	100	0.35
50	0.1	83.55	125	0.5
50	0.1	83.55	150	0.5
50	0.1	83.55	175	0.5
75	0.1	125.32	100	0.35
75	0.1	125.32	125	0.35
75	0.1	125.32	150	0.5
75	0.1	125.32	175	0.5
100	0.1	167.09	100	0.35
100	0.1	167.09	125	0.35
100	0.1	167.09	150	0.5
100	0.1	167.09	175	0.5

Note: Because a constant feed per tooth (f) was used, the feed rate (F) was only dependent on the cutting speed.

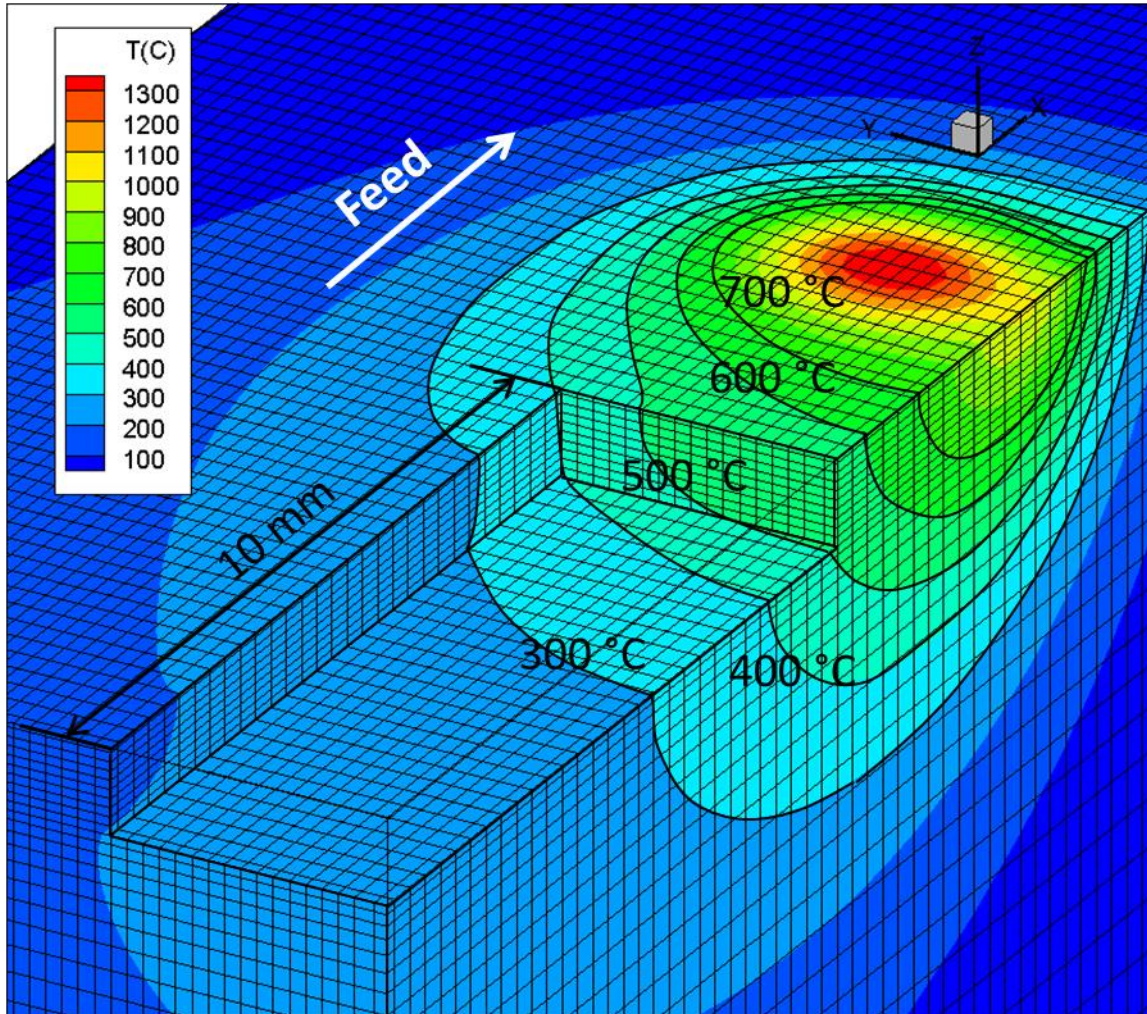


Figure 2.9: Thermal model example output for LAML of Ti-64.

In order to ensure that laser heating conditions were kept to appropriate levels, a regression analysis was performed to establish parametric relationships. MiniTab statistical software package was used to determine predictive equations based on the thermal modeling results, which could be used during LAML machining tests. The equations for T_{mr-ave} , T_{max} , and $T_{machined}$ were determined in terms of laser power (P), absorptivity of the fiber laser (α_f), and feed rate (F). By utilizing these equations, the needed laser power could be calculated using

the feed rate and appropriate absorptivity, based on the requisite surface temperature and experimental cutting conditions. Similar techniques have been used by others to predict workpiece temperatures (Dandekar et al., 2010). The work performed in the current study follows Wiedenmann et al. (2011) to ensure that a heat-affected zone is not created in the final workpiece material as a result of laser heating.

The resulting predictive equations from the regression analysis are given as follows:

$$T_{mr-ave} = 32.017 * \frac{(\alpha_f P)^{0.772}}{(F)^{0.156}}, \quad (2.8)$$

$$T_{max} = 133.238 * \frac{(\alpha_f P)^{0.633}}{(F)^{0.099}}, \quad (2.9)$$

$$T_{machined} = 94.492 * \frac{(\alpha_f P)^{0.721}}{(F)^{0.23}}, \quad (2.10)$$

where T_{max} is the maximum temperature under the laser beam, T_{mr-ave} is the average temperature in the material removal zone, $T_{machined}$ is the maximum temperature along the depth of cut (below the top surface), α_f is the laser absorptivity, P is the laser power and F is the feed rate.

From the thermal modeling results, it was determined that laser power close to 110 W would result in surface oxidation on the workpiece for the slow machining speeds of 37 m/min and 50 m/min. As a result, an appropriate workpiece absorptivity value of 0.5 was applied for a laser power level higher

than 110 W. It was determined that the final maximum machined surface temperature could exceed the 800°C temperature threshold needed for phase change to begin in a Ti-64 sample for laser power above 150 W. To ensure that phase change is not present on parts after LAML, 150 W was set as the upper limit for laser power when using slower machining speeds.

For the higher machining speeds of 75 m/min and 100 m/min, it was determined that laser power close to 140 W would result in oxidation of the workpiece surface; therefore, the corresponding absorptivity value of 0.5 was used for laser power above this value. From the modeling work it was determined that laser power above 185 W would result in 800°C threshold temperature on the final workpiece surface for a machining speed of 75 m/min. As a result, laser power was limited to 185 W and 200 W for 75 m/min and 100 m/min, respectively.

A summary of the modeling results is presented in Figure 2.10, with error bars representing the minimum and maximum temperature in the cutting zone. The dashed and broken lines respectively represent the critical temperatures in Ti-64 where phase change can begin (800 °C) and where surface oxidation begins (1100 °C). Based on the constraints established for the different machining speeds, it was observed that the surface of the final machined part could potentially be affected by the laser for T_{mr-ave} values above 475 °C. A maximum T_{mr-ave} of 500 °C was used in the tests to avoid possible microstructural change on the final surface of the part.

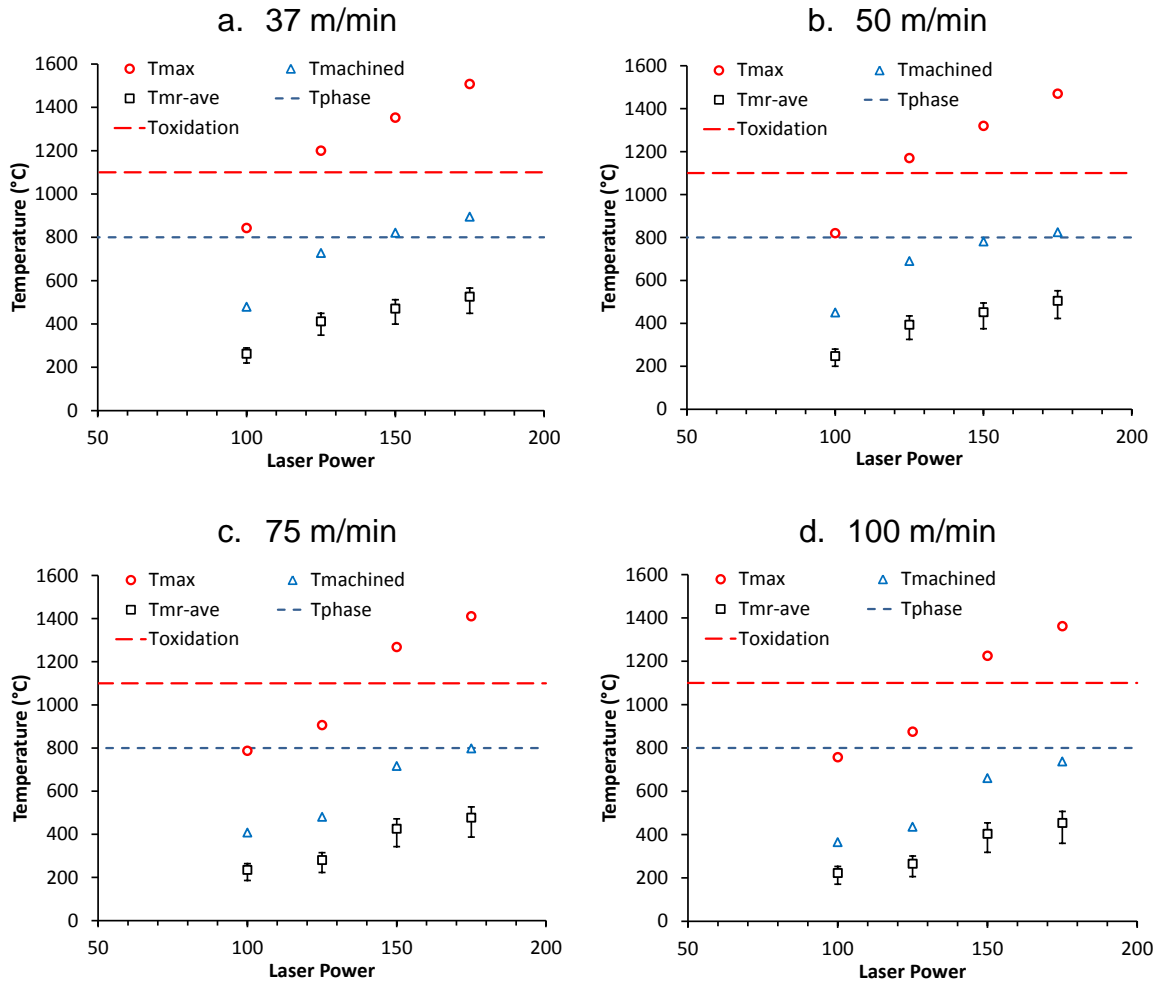


Figure 2.10: Thermal model simulation results for LAML temperature prediction.

2.2.5 Temperature Modeling of Material in Removal Zone

The thermal model uses a straight line for calculating the T_{mr-ave} temperature; however, more accurate results can be obtained from using the actual curved section generated due to the rotation of a cutting tool interacting with the workpiece. To determine what effect this change in material removal zone shape has on final T_{mr-ave} predicted temperatures, LAML modeling was performed using two techniques. The first technique captured the material

removal zone temperature using a straight line at the L_{lead} distance. For the second approach, a curved section along the workpiece surface was used to calculate temperatures in the cutting zone, shown in Figure 2.11.

Temperatures along the curve, down to the depth of cut, were averaged to determine the $T_{\text{mr-ave}}$ for the LAML process in the second approach. A weighted average method was used over the length of the curved line to account for changes in uncut-chip thickness during machining. When comparing the straight line material removal section with the curved section, it was found that there was less than 5% difference between the curved weighted average method and straight $T_{\text{mr-ave}}$ results. As a result, the $T_{\text{mr-ave}}$ calculation for a straight line was used to approximate the average temperature in the material removal zone.

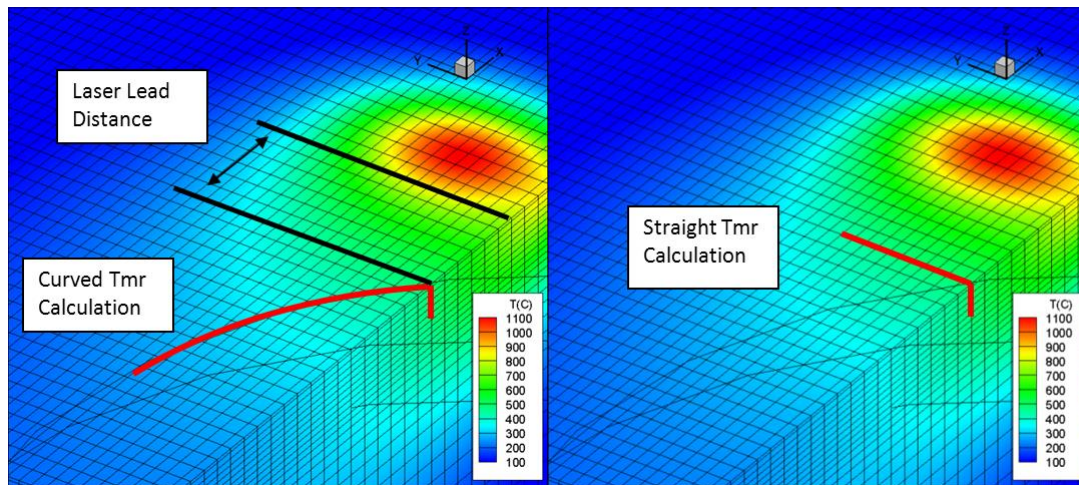


Figure 2.11: Images for curved and straight $T_{\text{mr-ave}}$ calculations.

CHAPTER 3. LASER-ASSISTED MILLING OF TI-64

This chapter presents the experimental results of both Ti-64 grade 5 and Ti-64 ELI grade 23 using conventional machining methods and laser-assisted machining techniques. This study on the machining of Ti-64 alloys included experimental investigation of cutting force and tool wear. Final workpiece properties are also investigated to determine what effect LAML has on phase composition, grain size, and surface hardness. An economic study is performed to determine the benefits of LAML when compared with traditional machining.

3.1 Ti-64 Grade 5

3.1.1 Experimental Design and Procedure

Experiments were performed using a face milling configuration. Machined passes were made in one direction with a specified distance (L_{lead}) between the edge of the laser beam and the cutting tool's entrance into the workpiece.

For machining experiments, a coordinate system was defined to relate the cutting forces measured by the dynamometer to the forces in the machining process. The feed direction was defined as the X direction, while the machining direction and width of cut was defined as the Y direction. The Z direction was defined as the axial direction and corresponded to the depth of cut used during

machining (Figure 3.1). Downmilling was used during machining and was defined by a larger chip thickness as the cutting tool entered the material, with a reduction in chip thickness over the remainder of the cut. For the Kennametal cutting tool, a tool diameter of 19 mm, feed of 0.1 mm/tooth, and depth of cut of 1 mm were selected based on typical machining parameters obtained from the literature, as discussed in the introduction. A KC520-grade carbide insert was selected for the experiments with Ti-64 grade 5. A width of cut of 3 mm was used in most experimental testing. Cutting force data from the dynamometer was recorded at a rate of 2 kHz.

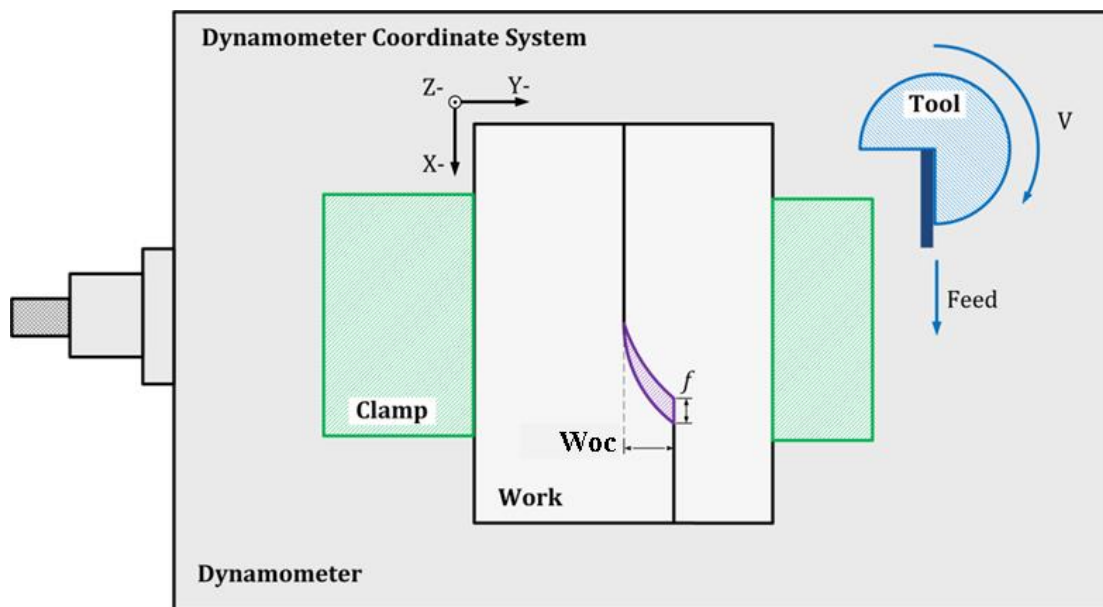


Figure 3.1: Machining coordinate system based on dynamometer.

3.1.2 Experimental Results and Discussion

3.1.2.1 Cutting Force

Experiments were performed, based on the machining parameters chosen, to determine the cutting force for different machining conditions using traditional machining and LAML. For an accurate representation of the maximum force during machining, the cutting force was calculated by using an average of the peak cutting force values along the length of cut. Traditional machining experiments were performed using three cutting speeds to determine the influence of cutting speed on overall cutting forces during machining.

From the measured results of traditional machining as shown in Figure 3.2, it was determined that cutting force did not change significantly in either the X or Y directions when comparing different cutting speeds for Ti-64 grade 5. The average peak cutting force for all cutting speeds in the Y-direction was found to be close to 315 N, while peak force in the X direction was close to 110 N for all machining speeds (Table 3.1). Variability of peak cutting force was determined over the length of the cut and standard deviation values were calculated for this length, as shown in Figure 3.2. From the results of this testing, a good baseline for cutting force was established for traditional milling.

Table 3.1: Cutting speed and force results for traditional experiments.

Speed (m/min)	Cutting Force	
	F _x -Peak (N)	F _y -Peak (N)
37	115	320
50	105	310
75	110	315

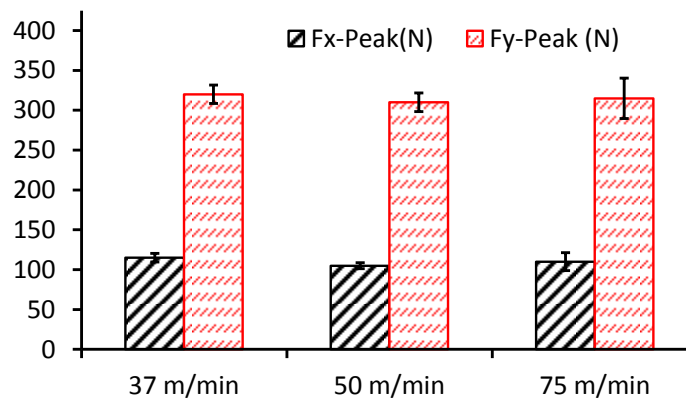


Figure 3.2: Cutting force measurements from traditional machining.

Cutting force was measured during LAML to determine the influence of laser power on final cutting force. A single machining speed of 50 m/min was chosen with a depth of cut of 1 mm and several laser power levels were tested. The details of the machining parameters used in the experimental design are shown in Table 3.2. Specifics for the laser parameters, which are based upon the beam delivery equipment, described in the experimental setup section of this report, are listed in Table 3.3. The laser power range was selected to keep the

final workpiece surface below the critical temperature for phase change; therefore, experiments were run with laser power between 75 W and 175 W.

Table 3.2: Experimental design for LAML of Ti-64.

Test	V (m/min)	Feed rate (mm/min)	f _{pt} (mm/tooth)	RPM	Laser	T _{mr-ave}	T _{max}	T _{machined}
					Power (W)	(°C)	(°C)	(°C)
Conv1	50	83.5	0.1	835.5	0	23	---	---
LAM1	50	83.5	0.1	835.5	75	200	679.1	360.6
LAM2	50	83.5	0.1	835.5	100	250	815.5	444.2
LAM3	50	83.5	0.1	835.5	127	300	947.0	526.6
LAM4	50	83.5	0.1	835.5	155	350	1074.7	608.2
LAM5	50	83.5	0.1	835.5	170	500	1439.9	848.7

Table 3.3: Invariant laser parameters.

Laser Spot Size	L _{lead}	L _{angle}	Assist Gas
(mm)	(mm)	(°)	
2.6x3.6	3.5	41	Argon

An example of averaged cutting force data recorded for 4 cycles during experiments is shown in Figure 3.3, where it can be seen that there is a significant reduction in peak cutting force for LAML, compared with traditional machining. A summary of the peak forces in both x and y directions for all the experiments is shown in Table 3.4, where it can be seen that cutting force

decreased in both X and Y directions as the laser power is increased. A graphical comparison in Figure 3.4 shows the general trend of reduced cutting force with increasing laser power, as well as the standard deviation.

This is an expected result when comparing modeling results with temperature-dependent strength properties of Ti-64 alloys. The best results were observed for LAML5 parameters, which resulted in a 50% decrease in peak cutting force in the x-direction, and a 30% decrease in peak cutting force in the y-direction. Based on the modeling work, a higher cutting force reduction would be expected for higher laser power, but these were not performed due to the consideration that alteration of final workpiece material properties would be detrimental.

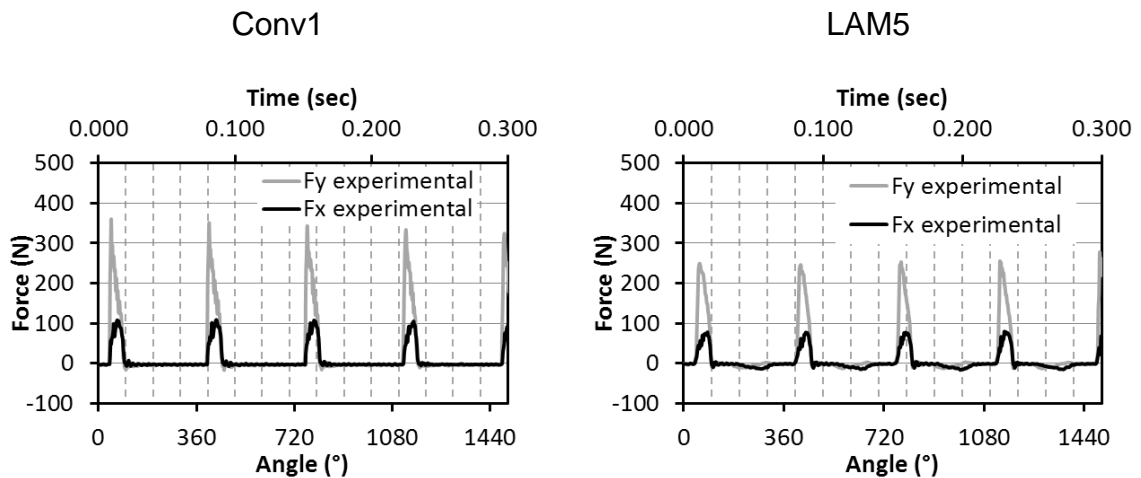


Figure 3.3: Experimental cutting force during multiple tool rotations.

Table 3.4: LAML experimental matrix and cutting force results.

Test	Power	T _{mr-ave}	F _{x-peak}	F _{y-peak}	% decrease-F _x	% decrease-F _y
Conv1	-	23	110	300	-	-
LAM1	75	200	105	295	5%	2%
LAM2	100	250	95	290	16%	3%
LAM3	127	300	90	270	22%	11%
LAM4	155	350	80	265	38%	13%
LAM5	170	500	73	235	51%	28%

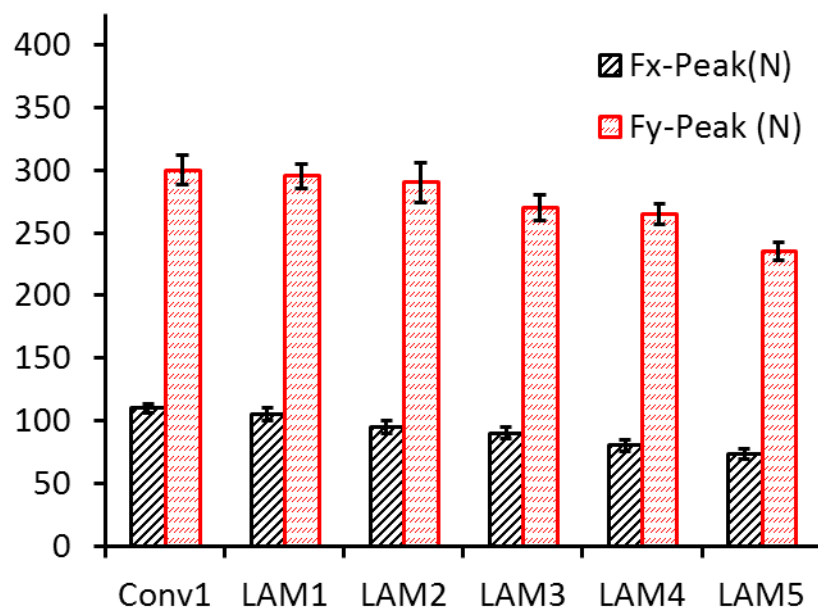


Figure 3.4: Average peak cutting force results with error bars for one standard deviation.

3.1.2.2 Tool Wear Analysis

Tool wear testing was performed using both traditional machining methods and LAML. Several machining speeds were chosen for this testing to determine total tool lives for traditional milling (without chipping) and LAML. Based on thermal modeling results and cutting force experiments, laser parameters were selected so as to avoid a potentially damaging phase change on the final workpiece surface. The laser power was selected for each cutting speed based on the regression analysis performed in the thermal modeling section of this report, to achieve a T_{mr-ave} value of 500 °C. A full list of experimental parameters is shown in Table 3.5.

Table 3.5: Tool Wear Experimental Parameters

Test	V (m/min)	RPM	fpt (mmpt)	P (W)	T_{mr-ave} (°C)
Conv-A	37	618	0.1	-	CONV
Conv-B	45	752	0.1	-	CONV
Conv-C	50	835	0.1	-	CONV
Conv-D	50	835	0.1	-	CONV
LAML-A	50	835	0.1	170	500
LAML-B	60	1003	0.1	175	500
LAML-C	75	1253	0.1	185	500

The tests for Conv-A through Conv-D were performed by progressively increasing machining speeds using a standard flood coolant and a KC520 insert.

Conventional testing at speeds higher than 50 m/min resulted in premature chipping of the insert during machining. As a result, the 50 m/min test was repeated to ensure the repeatability of tool life at this speed without the occurrence of premature chipping. LAML experiments were performed using the highest machining speed possible for conventional machining (50m/min), as well as higher cutting speeds up to 75 m/min. LAML testing was performed using an argon gas to prevent chips from either entering the laser optics or adhering to the cutting tool during machining.

An optical microscope was used to take images of the tool at different time increments during all machining experiments. The images were used to measure and record the flank wear present on the cutting tool (Figure 3.5). It is recommended by ISO 8688-1 that the tool should be rejected when the depth of chipping on the flank face or the width of chipping on the rake face is greater than 0.25 mm. To prevent potential damage to the experimental equipment, total flank wear greater than 220 μm from the edge of the initial tool geometry was used in this study to define total tool life. For experiments that resulted in premature chipping, this was observed to occur on both the flank and rake face of the cutting tool.

During LAML experiments it was observed that a thin layer of material would adhere to the cutting tool. This build-up of material did not have the typical characteristics of the built-up edge that occurs when machining other metals, and appeared as a thin coating over the cutting tool during machining. It was observed that this adhered material did not cause sudden chipping, which is

typical for machining that results in a built-up edge. Chemical composition of the thin layer was not tested; however, due to the chemical affinity of Ti to all other materials and the high temperatures present during LAML, it is expected that the majority of this material is Ti in composition. Traces of the thin build-up can be seen on the tool wear images shown in Figure 3.6 as a more reflective, or shiny, area on the LAML insert; however, this thin layer was typically scraped off using a fingernail in order to obtain accurate flank wear measurements.

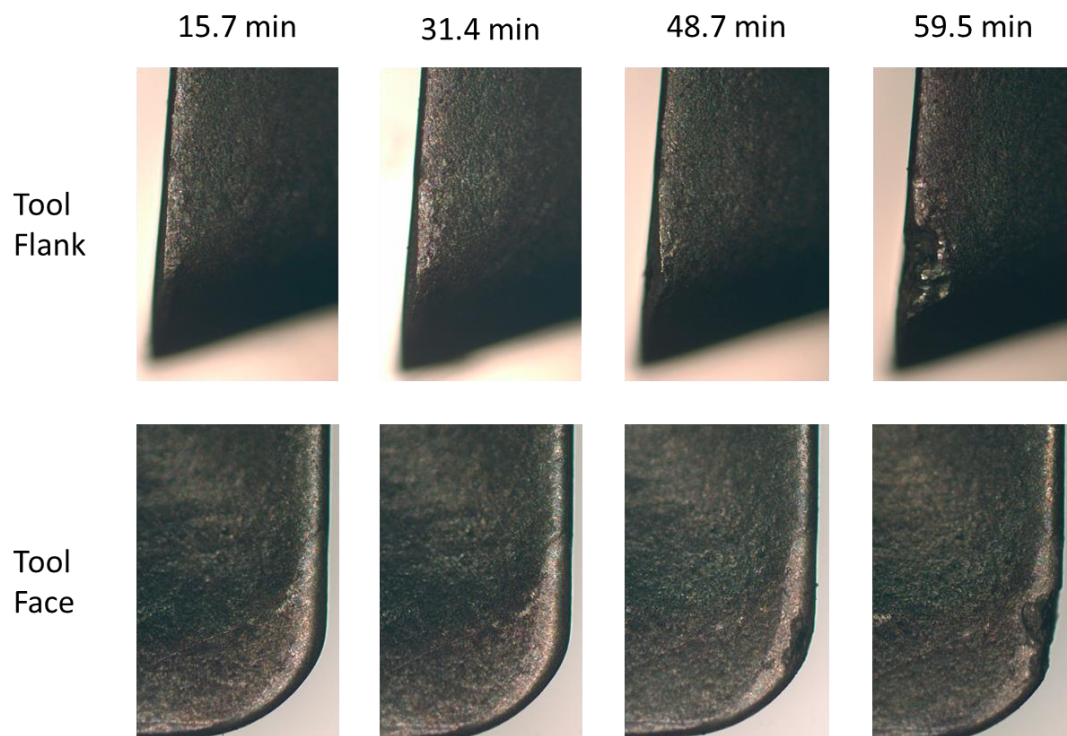


Figure 3.5: Tool wear images for CONV-B with KC520 insert.

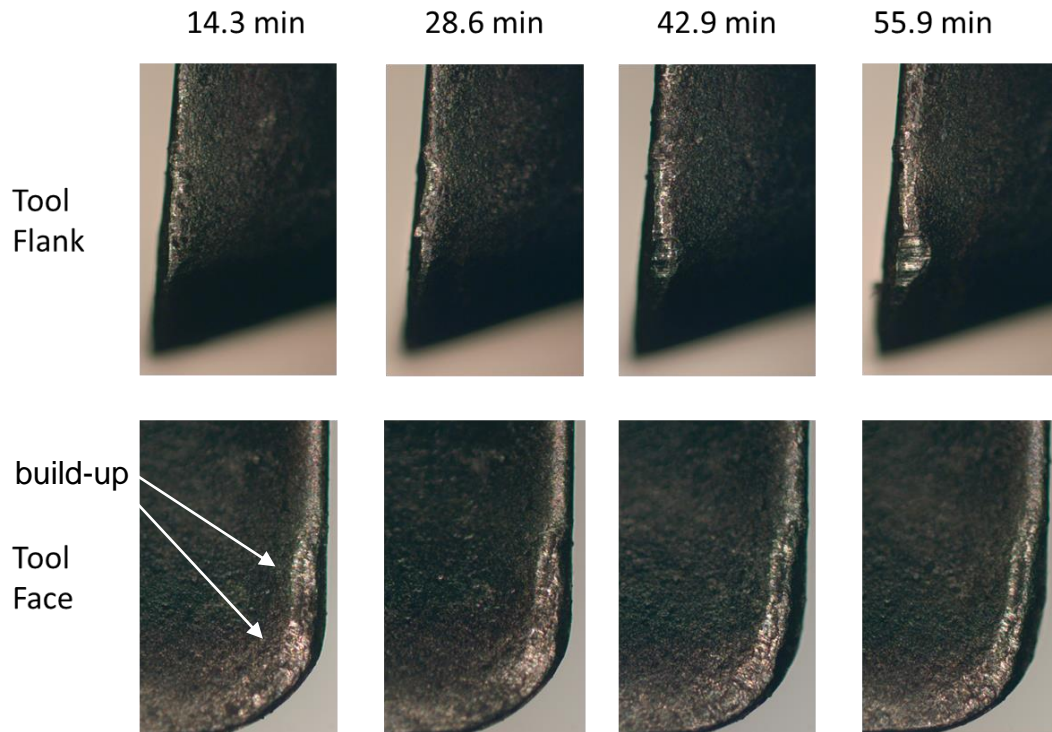


Figure 3.6: Tool wear images for LAML-B at 500 °C T_{mr-ave} with KC520 insert.

Nearly an equivalent tool life was achieved using LAML without a coolant at a cutting speed of 50 m/min as in traditional machining at 37 m/min with a flood coolant. As a result, cutting speed could be increased by 35% for LAML of Ti-64 grade 5, where the tool will spend the same amount of time removing material before it needs to be replaced. If an increase in cutting speed is not required, LAML can remove 35% more material than traditional milling over time before the tool must be replaced. Details of all the machining tests performed are shown in Figure 3.7.

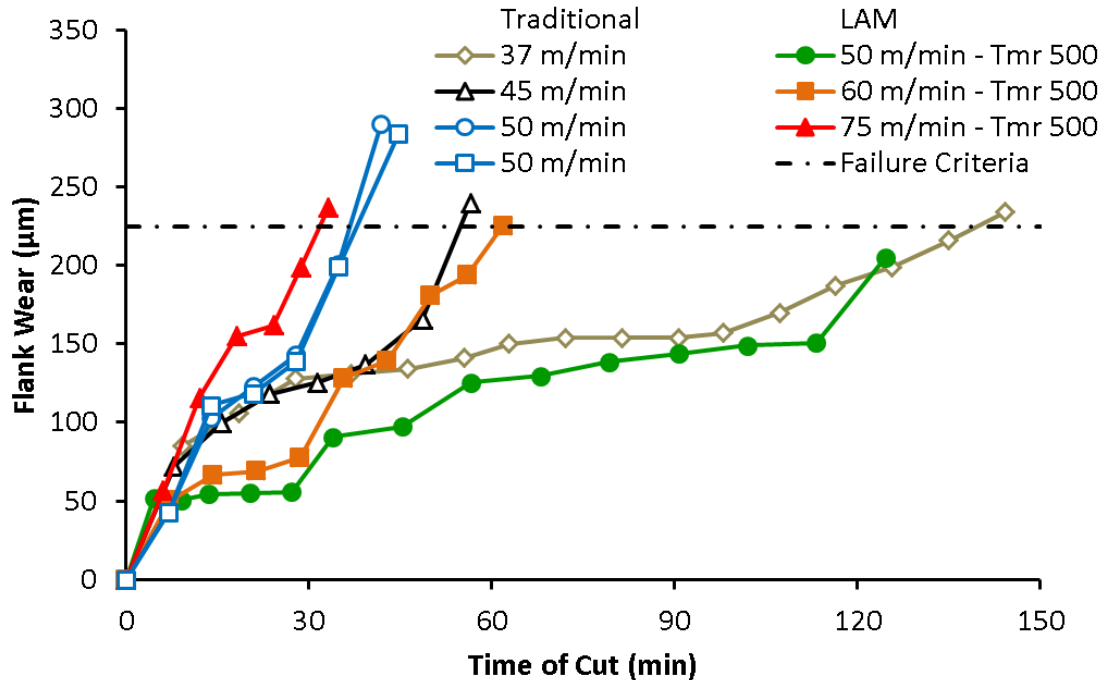


Figure 3.7: Ti-64 tool wear for traditional milling and LAML using a KC520 insert.

It is important to note that during testing LAML only uses an assist gas of argon to blow the chips off the tool and protect the laser optics from potential damage during machining. The direction of the assist gas to the tool is important because it ensures that the chips do not adhere to the tip of the tool after machining. It has been found that such chip adhesion can increase the tool wear rate (Sun, 2009).

From the cutting speed testing using traditional milling, where it was found that despite the increases in cutting speed there was little change in the measured cutting force, as insight can be provided into the premature tool chipping phenomenon during traditional milling. Typically, premature tool chipping occurs at a high cutting speed for Ti-64 machining. However, due to the

small difference in cutting force between different machining speeds, this chipping does not appear to be a direct result of cutting force changes. Therefore, it is expected that premature chipping results from several machining and material parameters that occur during the milling process. The LAML results of reduced cutting force, increased tool life, and elimination of premature chipping are of greater benefit than a pure reduction in cutting force for Ti-64 machining.

To accurately assess the benefit of LAML over conventional milling, predictive equations based on Taylor's tool life equation need to be established. Using the 220 μm failure criteria, total tool life was determined for each of the machining experiments. Based on these results, Taylor tool life equations were determined for traditional milling and LAML of Ti-64:

$$V_c * T^{0.225} = 112 \quad (\text{Traditional}), \quad (3.1)$$

$$V_c * T^{0.299} = 208 \quad (\text{LAML}). \quad (3.2)$$

A log-log plot of experimental tool life data and Taylor tool life equations for traditional machining and LAML is shown in Figure 3.8. The improvement in tool life by LAML is shown by the up shift of the trend line when comparing the two machining methods. The slightly lower slope indicates that the overall benefit of LAML continues at higher machining speeds.

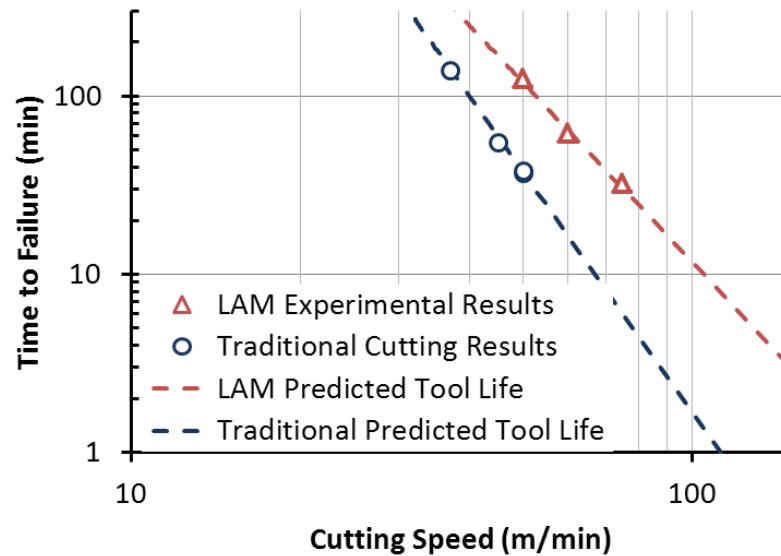


Figure 3.8: Taylor tool life equations for Ti-64.

3.1.2.3 Microstructural Analysis

It is essential that the final workpiece surface be characterized to identify changes in properties that can occur during machining. Due to the addition of heat from the laser to the workpiece surface, a heat-affected zone can potentially be created on the finished part. Although modeling was performed to obtain an appropriate laser power level based on material properties, machining parameters, and laser parameters, additional analysis was conducted to ensure that final workpiece properties were not negatively altered during the LAML process.

Images were taken using an optical microscope from the samples machined using Conv-C at 50 m/min and LAML-C at 75 m/min for the tool life experiments, which were then cross-sectioned and prepared using standard

metallographic techniques. A comparison of grain size and orientation beneath the machined surface was performed to determine what influence LAML had on final part microstructure. Based on observations of the cross-sectioned samples (Figure 3.9), it was found that there was no difference in grain size directly below the machined surfaces of any of the samples, and that the samples were similar down to a deep depth (>2mm). Grain orientation appeared to be random, with no specific orientation resulting from machining. Overall, no significant difference was observed between the two types of machining when optically comparing microstructures of the machined sample cross-sections. As in the case of Wiedenmann et al. (2011), modeling was successful to avoid a heat-affected zone on the final workpiece surface after LAML.

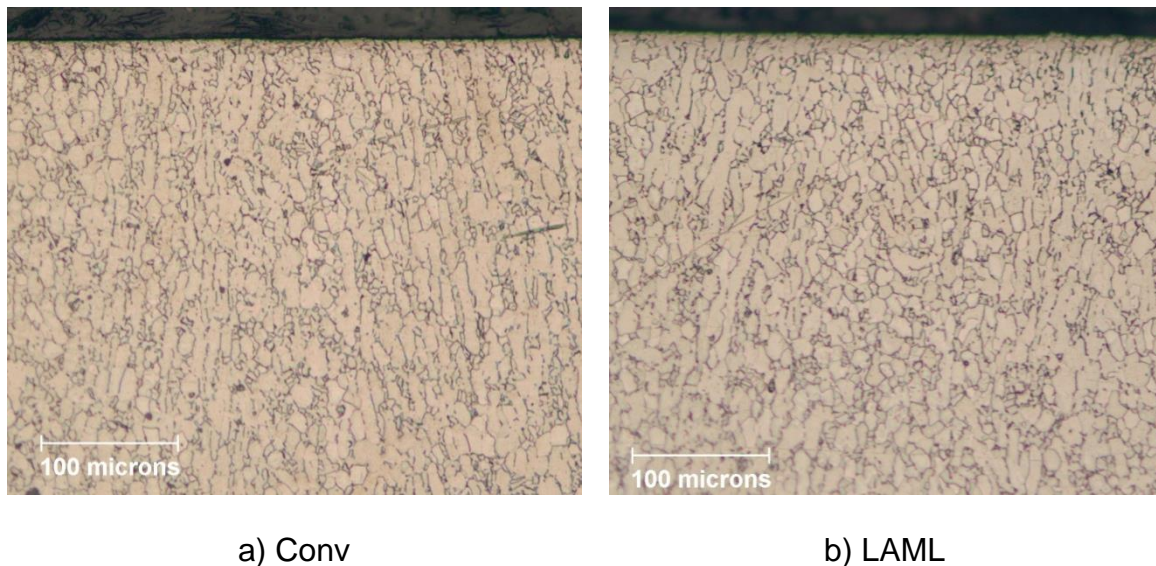
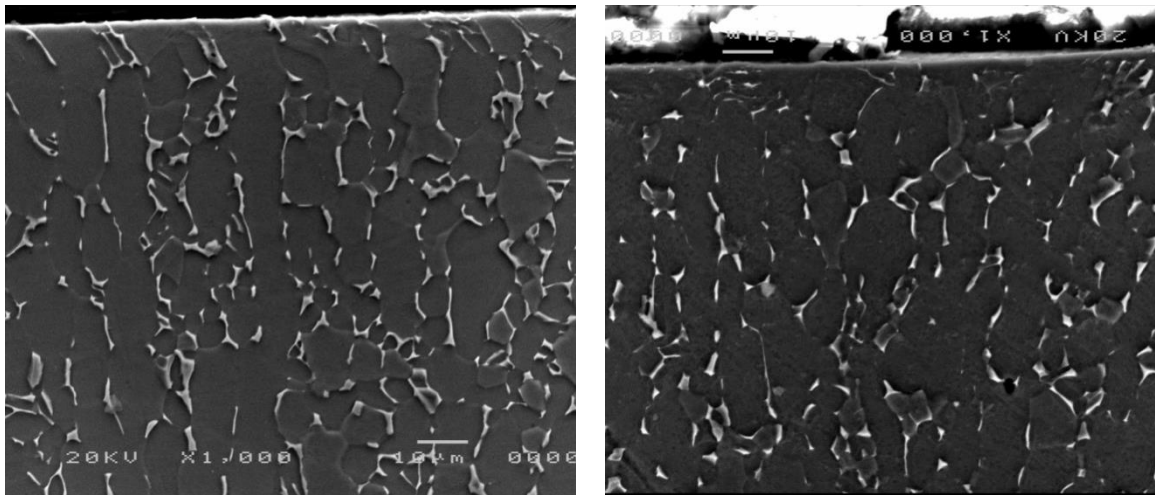


Figure 3.9: Ti-64 optical microscope images from cross-sectioned samples etched with Kroll's reagent at 200x after traditional machining (a) and LAML (b).

SEM images were taken and compared between traditional milling and LAML samples in order to make a better comparison of grain size and orientation

of the Ti-64 samples. The SEM images obtained are consistent with other images from literature (Chandler, 1989) for an AMS 4911 plate of Ti-64 grade 5. From a microstructural comparison it was found that there is no clear difference in grain boundaries between the two cases for the α -phase present, and that a microstructure of equiaxed α with a small amount of intergranular β is present through the entirety of the part (Figure 3.10). By observing the cross-section of the material, it was determined that there was not a significant change in material composition from the top of the machined surface all the way to the bulk of the material (>2 mm). As a result of optical microscope and SEM images, it can be concluded that LAML process parameters chosen did not produce a heat affected zone in the final workpiece.



a) Conv

b) LAML

Figure 3.10: SEM images of etched Ti-64 sample at 1,000x after traditional machining (a) and LAML (b).

Because Ti-64 is a heat-treatable alloy, material properties of the workpiece can change when it is irradiated by a laser. For cases without material removal, a laser has been used successfully to change an α -phase Ti workpiece with a small amount of β -phase into a predominantly β -phase Ti with a small amount of α -phase in the areas of the workpiece under laser irradiation (Hahn et al., 2007). Such phase changes can be beneficial, or detrimental to the final workpiece, depending on the specific needs of a component. To generally characterize the improvement that can be achieved during LAML, and based on the specifications for an AMS 4911 plate which is provided in an annealed state, it was assumed that a phase change on the final workpiece would have a detrimental impact on final part properties. Laser power levels were limited to ensure that temperatures did not exceed the critical cutoff for phase change based on the maximum temperatures predicted by thermal modeling.

The current thermal model only considers temperature changes resulting from laser irradiation onto the workpiece surface and overall heat flow due to convection, conduction, and radiation. It does not account for additional heating of the workpiece in the material removal zone, which results from plastic deformation and friction during the milling process (as shown in Figure 3.11). As a result, final workpiece surfaces must be tested to determine if final part properties have been modified during machining. Non-destructive surface inspection using XRD analysis was performed on machined parts. This analysis was used to determine which phases are present after machining using

traditional milling and LAML. Samples used in the XRD analysis did not receive special preparation and had an average surface roughness of $0.3 \mu\text{m}$.

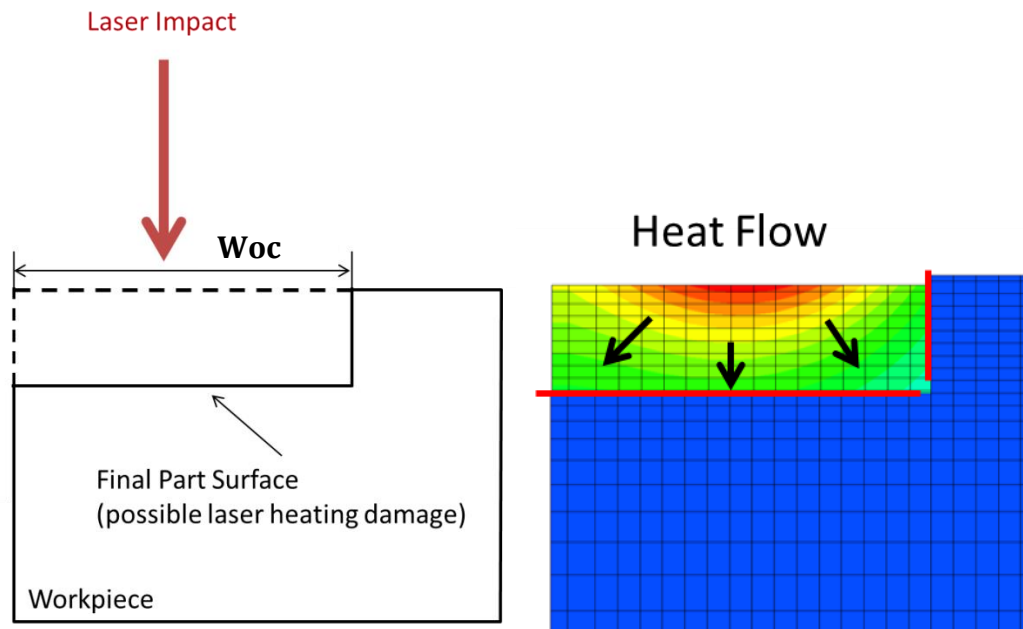


Figure 3.11: Temperature profile in workpiece with laser scan and feed into page.

According to literature (Vreeling et al., 2002; Gülerüz et al., 2004; da Silva et al., 1999), the standard way to characterize the 2θ peaks in Ti-64 is to use the Joint Committee on Powder Diffraction Standards (JCPDS) for titanium. The hexagonal α -Ti and cubic β -Ti from the JCPDS standard (file #44-1294, and #44-1288, respectively) were used to determine where peaks should occur. Measurements were taken on the workpiece surface, and this experimental data is plotted with reference points for the XRD phase standards of Ti-64 (Figure 3.12).

From a comparison of measured peaks to reference points, it can be seen that the machined surface mainly consists of α -phase Ti after traditional

machining. Since there are no significant peaks present for the β -phase Ti on the LAML sample, it can be concluded that machining with the laser will not induce a phase change, as long as appropriate laser power is used to perform LAML. This indicates that thermal model predictions can be used to accurately determine maximum laser power to enhance machining of the material, without exceeding the critical threshold temperature for Ti-64 grade 5 during LAML. This conclusion is reinforced through the images from the SEM, which show no significant change in grain size and orientation at the machined surface as well as within the bulk material.

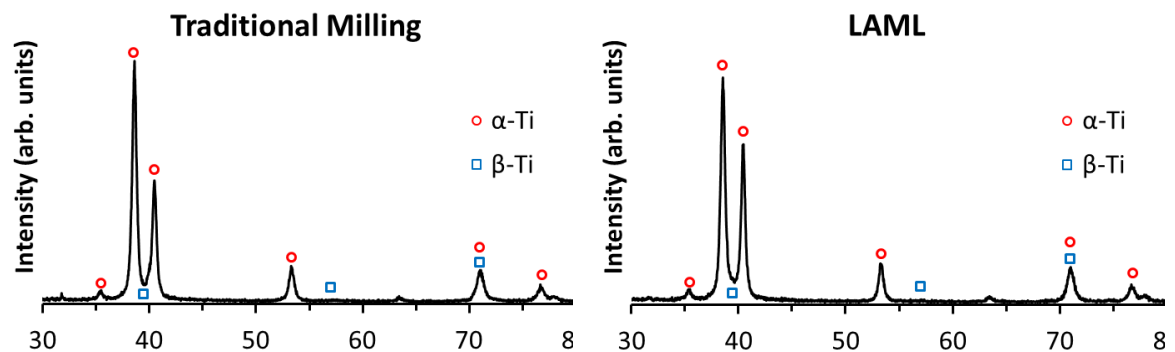


Figure 3.12: XRD analysis for milling Ti-64.

A Mitutoyo hardness tester (model ATK F1000) was used to determine the surface hardness of samples from the original Ti-64 material, traditional machining, and LAML. Each sample was tested 8 times and the results are shown in Figure 3.13. The error bars included are for one standard deviation of the measurements.

From these measurements, it was determined that there is a very slight decrease in the surface hardness of the final part. However, this is not a result of a detrimental phase change, based on the XRD analysis performed. During traditional machining there can be an increase in surface hardness from grain size refinement and increased residual stresses during plastic deformation and the shearing process. It has been shown that compressive residual stresses are generally observed during the milling of titanium (Mantle and Aspinwall, 2001; Sun and Guo, 2009). This increase in compressive residual stress can result in an adverse reduction of ductility at the surface of the part.

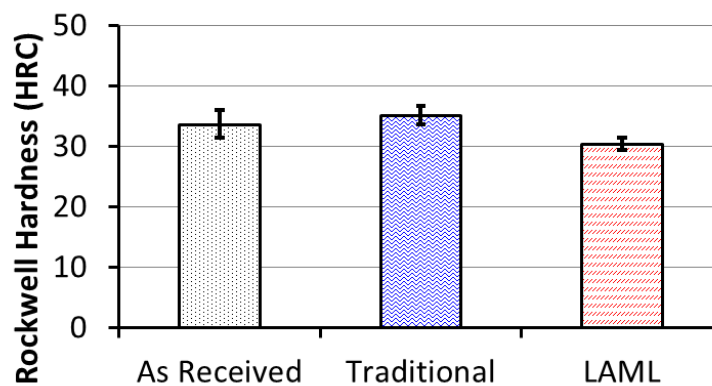


Figure 3.13: Ti-64 surface hardness results for the as-received material, Conv-C at 50 m/min and LAML-C at 75 m/min.

The measured surface hardness was reduced by less than 10% for the LAML samples when compared with traditional machining. As a result, final hardness measurements were within the range of the as-received material for hardness. The overall measured variations of final surface hardness for both types of machining were greatly reduced, when compared with those of the as-received material.

Due to the measured reduction in surface hardness, a detailed investigation into microhardness was performed to determine if there was a significant alteration in hardness beneath the surface of the LAML workpiece. Microhardness analysis was performed on cross-sectioned samples for Conv-C at 50 m/min and LAML-C at 75 m/min using a LECO KM 247AT machine.

Microhardness was analyzed at intervals of 100 μm for each sample down to a depth of 2mm, with an additional data point at 50 μm . Hardness closer to the workpiece surface could not be measured accurately, as the workpiece would deform when the indenter was too close to the edge.

It was determined that there was a relatively consistent hardness for both LAML and traditional machining, and that this hardness did not significantly change through the depth of the workpiece. Close to the surface of the workpiece, a slight increase in hardness was observed for both LAML and traditional machining experiments, indicating that the surface hardness differences measured were very shallow with respect to the top of the workpiece surface (Figure 3.14). Consequently, there was not a detrimental decrease in hardness of the workpiece as a result of LAML when compared with the bulk workpiece material, and surface hardness measurements fell within the acceptable range for Ti-64 grade 5 based on AMS 4911 specifications.

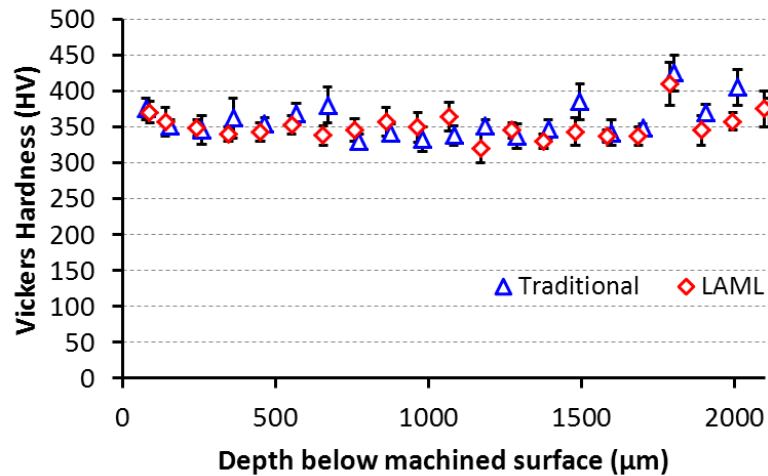


Figure 3.14: Microhardness results for Conv-C and LAML-C.

Residual stress analysis was performed on the machined samples for Conv-C at 50 m/min and LAML-C at 75 m/min. Measurements were taken from the machined surface of the sample in the feed and machining directions. The surface was etched and additional residual stress measurements were taken to a depth of 200 μm where stresses returned to zero.

It was found that there was a slight reduction in compressive residual stress on the surface of the workpiece as a result of the different machining processes. The reduction from LAML was close to 10% in both directions, which is consistent with the measured results of final workpiece surface hardness. Comparisons of residual stress data for traditional milling and LAML in the machining and feed directions are shown in Figure 3.15.

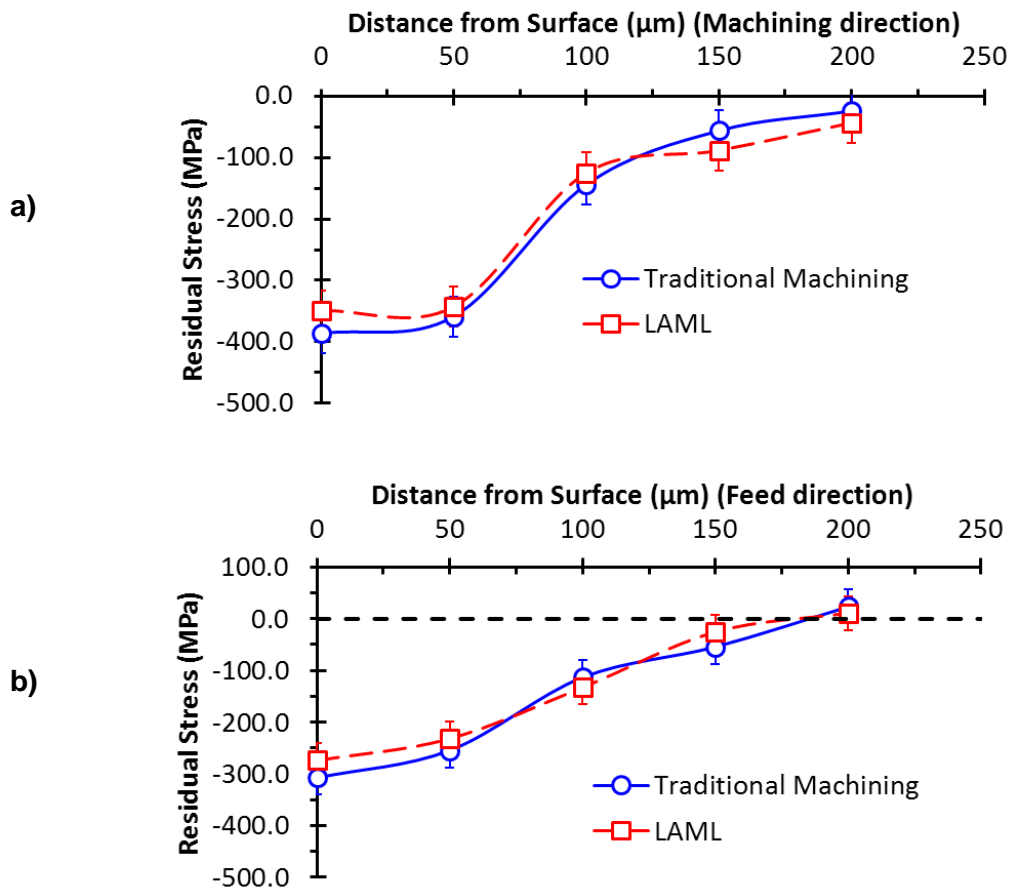


Figure 3.15: Residual Stress measurement for Ti-64 after Conv-C and LAML-C for machining direction (a) and feed direction (b).

When comparing the results of the residual stress with surface hardness and micro-hardness measurements, it is clear that LAML induces less residual stress onto the workpiece during machining, resulting in a slight decrease in surface hardness. This is perhaps due to the reduced cutting force, or stresses induced during LAML. The reduced residual stress only affects a very shallow portion of the machined workpiece and does not affect workpiece properties at deeper depths (below 200 μm).

From all of the microstructural analysis performed on the final workpiece, it can be concluded that LAML machining can be implemented with parameters that do not negatively influence final workpiece properties. Laser parameters can be calculated prior to machining experiments using thermal modeling predictions for a workpiece. This allows the process to increase tool life and machining speeds while avoiding negative effects of laser heating during the LAML process. It was also determined LAML allows for the implementation of higher machining speeds without affecting final part properties.

3.1.3 Economic Analysis

To characterize the benefits that result from LAML, an economic analysis was performed for both traditional milling and LAML based on tool life predictions. Cost savings can be calculated for the increase in tool life achievable in LAML. The analysis uses the following assumptions for operating conditions and associated costs:

- \$200 per hour operation cost rate
- 7 min tool change time
- Tool cost: \$17 per insert – 2 cutting sides (\$8.50 per tip)
- Part size: 4,000 mm³ (amount of material removed per part)
- At least one part made per tool
- Laser operation cost: \$30 per hour for operation & depreciation

From the assumptions given and the Taylor tool life equations obtained from experimental testing, the total cost per piece was plotted for different cutting

speeds during traditional machining with a coolant and LAML (Figure 3.16). Since premature chipping does not occur during LAML, higher speeds are possible for part fabrication. As a result, LAML can be performed at speeds that are optimized based on total machining costs.

The optimum cutting speed to minimize cost and maximize productivity was calculated for both traditional machining and LAML (Table 3.6). These values were determined by balancing material removal rate and tool life to produce the lowest cost per part, or maximum part production. The calculated total cost for traditional machining using a cutting speed of 50 m/min is highlighted in Figure 3.16a, with premature chipping occurring at cutting speeds above 50 m/min, as indicated. The minimum cost for LAML is highlighted in Figure 3.16b. The potential increase in machining speed can be clearly seen when comparing the two charts, and a reduction in cost per piece is also observed.

Table 3.6: Optimized cutting speed from Taylor tool life equations.

Machining Type	Optimized cutting speed	
	Min-cost (m/min)	Max-productivity (m/min)
Traditional	50	54
LAML	85	90

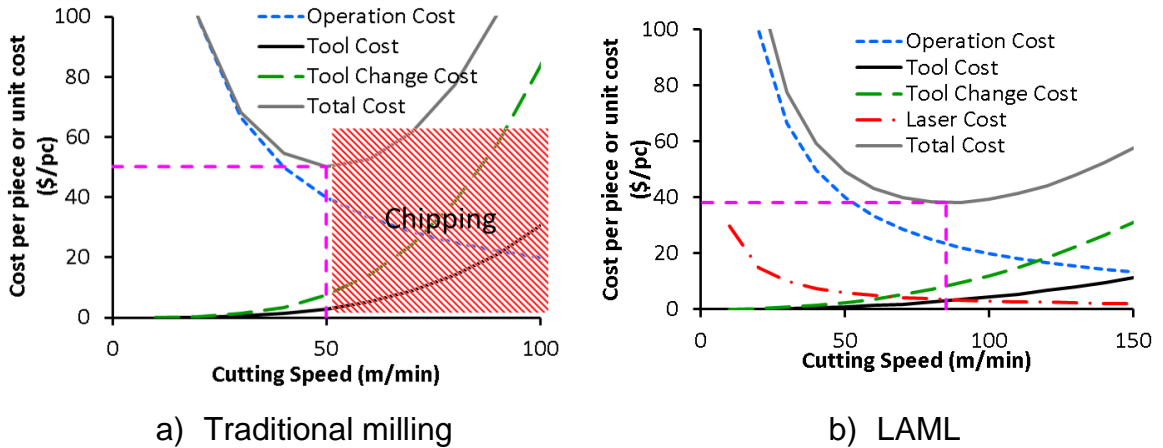


Figure 3.16: Cost of producing one part based on Taylor tool life equations.

The total machining cost for machining one part is calculated for the optimum cutting conditions, with costs separated into their sources (laser, tool change, tool cost, and operational cost) as shown in Figure 3.17. As evidenced in the table, there is a 33% reduction in cost for producing parts using LAML, even when accounting for the costs of the laser operation. Laser operational costs include powering the laser and chiller, supplying an assist gas, and depreciation of equipment over time.

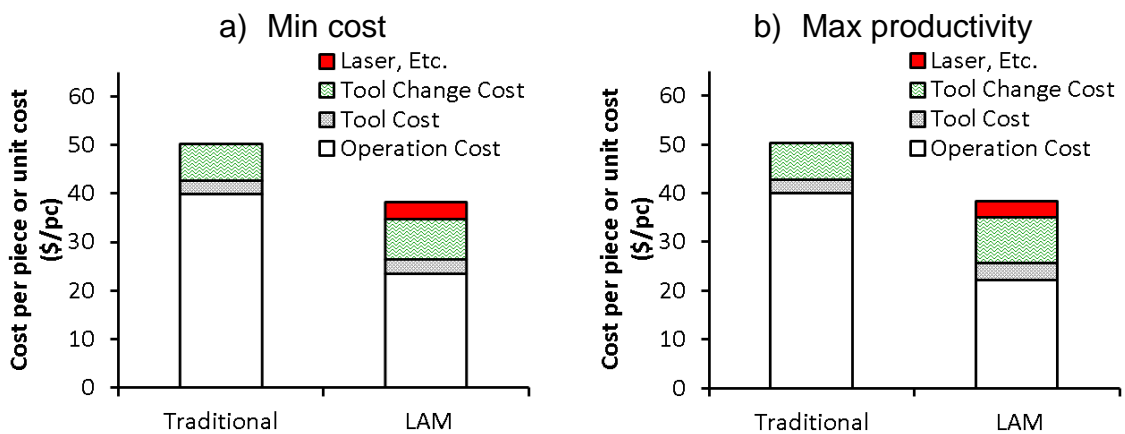


Figure 3.17: Machining costs for optimized traditional machining and LAML.

Comparisons of material removal rates have also been performed for current cutting practices and LAML using optimum parameters (Figure 3.18). LAML can produce parts with a much higher material removal rate such that two parts can be produced for every part made using traditional milling. This is a significant productivity improvement over the current manufacturing method, and comes with a reduced cost per part.

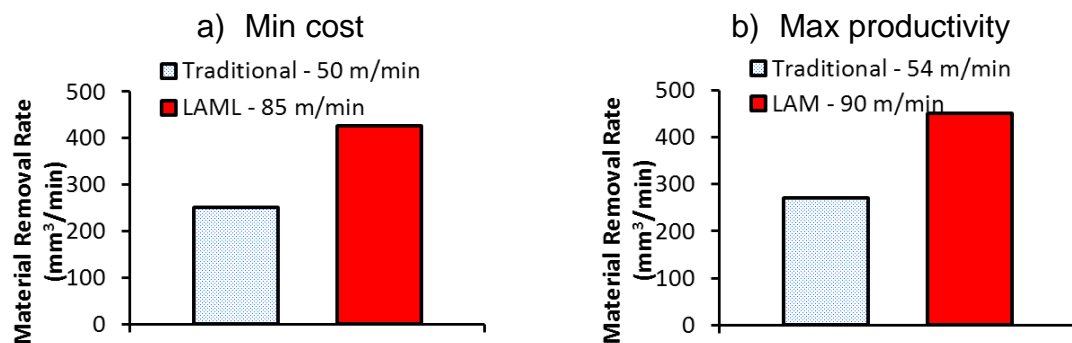


Figure 3.18: Material removal rates for traditional machining and LAML.

One significant benefit of LAML over traditional milling, which is not considered in this economic analysis, is the impact of a coolant during machining. Since LAML does not require traditional coolants during the machining process, there can be added economic savings. There is also a direct environmental impact from the elimination of coolants since they do not need to be processed after they are no longer useful. It should be noted that there are additional safety benefits provided to workers operating the equipment without use of a coolant; however, it is recognized that safety precautions are needed for successful implementation of LAML.

3.2 Ti-64 ELI grade 23

3.2.1 Experimental Design and Procedure

Experiments were performed using a face milling configuration for traditional machining and LAML. Details of the machining coordinate system are outlined in the Ti-64 grade 5 experimental design section included in this report. The Ti-64 ELI grade 23 workpiece size had dimensions of 150x125x50 mm³. Each cutting pass had a machining length of 150 mm. A Kennametal cutting tool was used which has a tool diameter of 19 mm. A KC725M grade TiAlN PVD-coated carbide insert was used during machining.

3.2.2 Experimental Results and Discussion

3.2.2.1 Cutting Force

A cutting speed of 75 m/min was used during machining experiments to characterize the influence of laser heating on cutting force, so that an accurate comparison could be made between traditional machining and LAML when using a face milling configuration. During the machining experiments, cuts were made along a Ti-64 ELI sample with dimensions of 150x125x50 mm³, with machining occurring along the 150 mm length. Machining parameters used included a 75 m/min cutting speed, 0.1 mm feed per insert, 1 mm depth of cut, and 3 mm width of cut. Laser parameters included a 2.6x3.5 mm² laser spot diameter with an elliptical shape, 3.5 mm laser lead distance, and a 41° angle of incidence

measured from horizontal. Tests were performed with and without laser heating of the workpiece, as detailed in Table 3.7.

To avoid potential phase change in the final workpiece surface, a laser power of 180 W, based on the thermal modeling and regression analysis, was used during LAML. It was determined that this power would not increase the temperature at the final depth of cut location beyond the chosen critical cutoff temperature for phase change, (800 °C) for an area of the workpiece larger than 100 μm in the axial or radial directions. Based on the laser parameters, it was calculated that machining would be carried out with a $T_{\text{mr-ave}}$ of 500 °C.

Table 3.7: Experimental Design for LAML of Ti-64.

Test	V (m/min)	Feed rate (mm/min)	Feed (mm/tooth)	RPM	P (W)	$T_{\text{mr-ave}}$ (°C)	T_{max} (°C)	T_{machined} (°C)
Conv	75	83.5	0.1	1253	0	23	---	---
LAML	75	83.5	0.1	1253	180	500	1500	780

Cutting force was recorded at 2 kHz. Peak force data was taken over the total length of cut, and an average peak cutting force was determined for each experiment. A summary of the peak cutting force in both X and Y directions for each experimental condition is listed in Table 3.8. It was found that laser heating reduced forces by 23 and 20 percent in the Y and X directions, respectively, as shown in Figure 3.19, with error bars representing one standard deviation in cutting force. From the LAML experiments it is clear that localized heating of the workpiece material reduces the cutting force required during the machining

process. The small cutting force observed between cycles was a result of tool rubbing against the workpiece surface, which is common during milling operations.

Table 3.8: Experimental Matrix and Results of Milling of Ti-64.

Test	P (W)	T _{mr-ave} (°C)	F _{x-Peak} (N)	F _{y-Peak} (N)	F _x % decrease	F _y % decrease
Conv	-	-	120	333	-	-
LAML	180	250	100	270	20	23

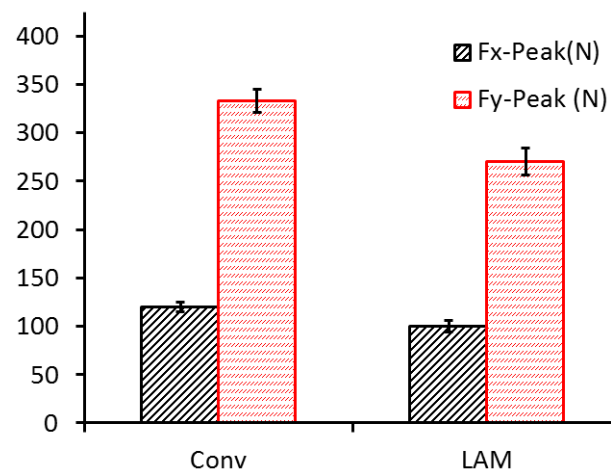


Figure 3.19: Average Peak Cutting Force Results – error bars for one standard deviation.

The 20% reduction in cutting force measured during LAML of Ti-64 ELI is not as large as the 60% reduction observed during milling of Inconel 718 (Brecher et al., 2010) or the 40% reduction during milling of a Ti-64 alloy (Sun et al., 2011). This is primarily a result of differences between laser power and

configuration during machining. Because material properties of the final workpiece surface were of critical importance for the Ti-64 alloy, and the material is heat-treatable by nature, laser power was limited during this study. This consideration is not included in the work presented by Brecher et al. (2010) and Sun et al. (2011), therefore, with a higher laser power, a larger reduction in cutting force could be expected.

Beam placement can also be a driving factor for the reduction in cutting force. The position of the laser relative to the cutting tool will influence the final temperature profile within the workpiece. As a result, temperatures within the cutting zone can be significantly different, which directly impacts the final cutting force occurring during machining. For this study, the more standard approach of applying the laser to the workpiece ahead of the cutting tool was used, instead of the novel concept of laser integration through the spindle (Brecher et al., 2010).

3.2.2.2 Tool Wear Analysis

Tool wear tests were performed on the Ti-64 ELI workpiece using the KC725M grade coated carbide insert. Conventional milling tests were performed using a traditional cutting speed for titanium alloys of 50 m/min, as well as higher speeds (65 and 75 m/min) to establish a baseline for overall tool life. A flood coolant was used at all speeds. It was found that traditional milling at cutting speeds above 50 m/min would result in premature chipping of the tool during Ti-64 ELI machining. As discussed in the Ti-64 grade 5 section of this report,

premature tool chipping is quite common when machining titanium alloys at high cutting speeds and can reduce the predictability of tool life.

Because premature tool chipping can result in catastrophic tool failure during part production, conventional milling experiments were performed only until chipping was apparent on the tool. It is recommended by ISO 8688-1 that the tool should be rejected when the depth of chipping on the flank face or the width of chipping on the rake face is greater than 0.25 mm; however, to prevent potential damage to the experimental equipment, a critical cutoff value of 180 μm was used to define flank wear for the tool. This value minimized the role of chipping in overall tool life so that accurate tool wear trends could be calculated.

LAML experiments were performed on the Ti-64 ELI workpiece without a coolant at a cutting speed of 75 m/min and 100 m/min to determine the effect of LAML on overall tool life. Argon gas was applied in experiments to remove chips from the tool and to protect the laser optics from potential damage. A total flow rate of 0.47 lpm at 0.35 MPa was delivered using two nozzles. Machining parameters used in tool wear testing were the same as those described in the cutting force experiments of Ti-64 ELI, with cutting speed and laser power modified based on the modeling work and regression analysis performed. For tool life experiments, both traditional machining (Conv1-Conv3) and LAML (LAM1-LAM2) were performed for machining speeds between 50 m/min to 100 m/min. A concise summary of machining parameters is listed in Table 3.9.

Table 3.9: Tool Wear – experimental parameters.

Test	V (m/min)	RPM	f_{pt}(mmpt)	P (W)	T_{mr-ave} (°C)	Coolant
ConvA	50	835	0.1	-	CONV	Oil based
ConvB	65		0.1	-	CONV	Oil based
ConvC	75	1253	0.1	-	CONV	Oil based
LAMA	75	1253	0.1	185	500	None
LAMB	100	1671	0.1	195	500	None

Unlike traditional machining, chipping was not present on tools machined using LAML at high cutting speeds. The elimination of premature chipping at high speeds is a significant improvement for LAML compared with traditional milling. Testing was performed for LAML experiments until 225 μm of flank wear was measured. In order to accurately compare total tool life between LAML and traditional milling, the lower critical value for flank wear of 180 μm was used to define total tool life. Machining was performed for a set amount of time at each machining speed with tool wear recorded for total flank wear observed on the insert (Figure 3.20).

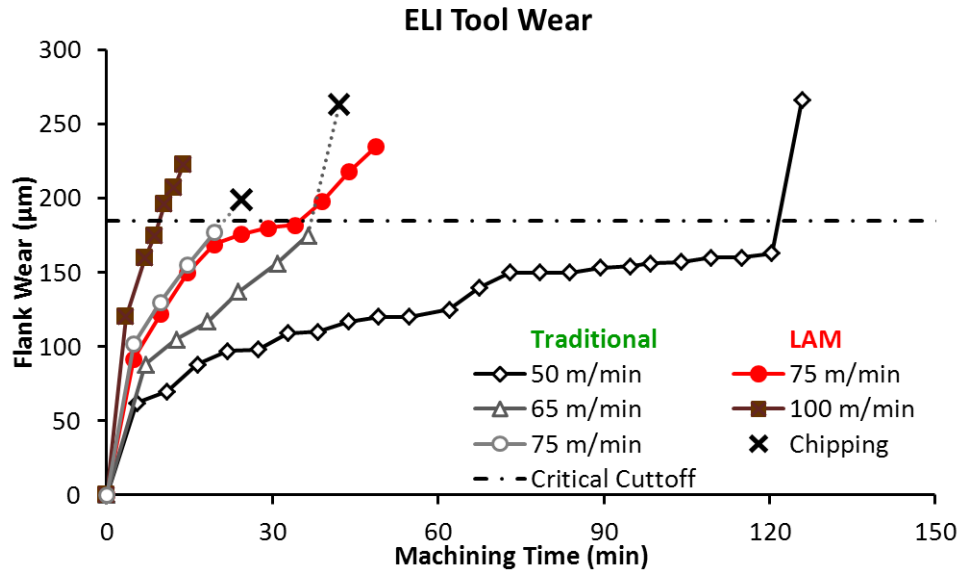


Figure 3.20: ELI Tool Wear – 725M Insert.

As shown in the results for tool life testing, there is a clear improvement when using LAML over traditional machining. The two main improvements measured were slower progression of flank wear on the tool and the elimination of chipping at high cutting speeds during LAML. Due to the increased tool life, an insert used with LAML will last 64% longer than one used with traditional milling. Alternatively, the cutting speed for traditional milling can be increased by 30% when using LAML, without reducing the total tool life of the insert. This increase in cutting speed is feasible due to the elimination of chipping at higher cutting speeds during LAML. Both of these benefits can have a significant impact on part production time and total cost.

Brecher et al. (2010) found that LAML of Inconel 718 resulted in significantly reduced cutting force and tool wear. During machining tests at 75 m/min, using 1000 mm³ of removed material, 140 µm and 60 µm of flank wear

were present for traditional machining and LAML, respectively. This is significantly better than the results of the current work; however, laser power considerations must be taken into effect. Inconel 718 is not a heat-treatable material, and hence, a much higher laser power could be employed during their study. As a result, much larger cutting force reduction and improvement in tool life could be achieved during LAML of Inconel 718 by Brecher et al. (2010). It must be noted that laser parameters used during this study, for the LAML of Ti-64, are not necessarily optimal because the study focused on tool life testing. It is conceivable that greater tool life improvements may be achievable through a modification of laser parameters including spot size, lead distance, laser power, and beam placement.

To compare overall tool life for traditional milling and LAML, the Taylor tool life equation was used to characterize failure of the tool as a result of flank wear. Failure of the tool was defined by flank wear that had exceeded 180 μm for a predictable tool life at all cutting conditions without premature chipping. This value is lower than the standard 200 μm , typical for Ti tool wear; however, it ensures that accurate values are obtained for all tool life tests performed.

Using the 180 μm flank wear criteria, a Taylor tool life equation was determined for both traditional milling and LAML of Ti-64 ELI:

$$V_c * T^{0.22} = 112 \quad (\text{Traditional}), \quad (3.3)$$

$$V_c * T^{0.22} = 168 \quad (\text{LAML}). \quad (3.4)$$

For comparison, a log-log plot was created that shows experimental tool life alongside the Taylor tool life equations, which were calculated for traditional

machining and LAML (Figure 3.21). As it was observed with Ti-64 grade 5 experiments, Ti-64 ELI grade 23 has an increase in machining time during LAML, as can be seen by the up shift in the time-to-tool-failure on the graph.

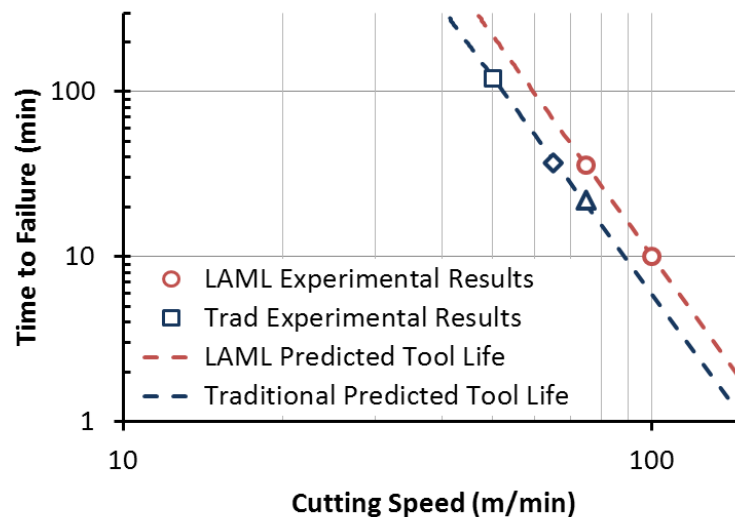


Figure 3.21: Taylor tool life equations and experimental data for Ti-64 ELI.

3.2.2.3 Microstructural Analysis

It is essential that the final workpiece surface of Ti-64 ELI grade 23 be characterized to identify changes in properties that can occur during machining. The addition of heat from the laser to the workpiece surface introduced the potential for a heat-affected zone on the finished part. Although modeling was performed to obtain an appropriate laser power based on material properties, machining parameters, and laser parameters, additional analysis was performed to ensure that final workpiece properties were not significantly altered during the LAML process for this alloy.

Workpieces were cross-sectioned and images were taken for the machining test conditions of ConvA and LAMA, which had a cutting speed of 50 m/min and 75 m/min, respectively. A higher machining speed for LAML was used in the comparison to ensure that the increased speed did not alter workpiece parameters beyond what is achieved during traditional milling at common cutting speeds. Acceptable resultant material properties would indicate that increased cutting speeds, as well as the laser surface heating, do not negatively influence final part properties.

A comparison of grain size and orientation beneath the machined surface was made to determine what impact LAML had on final part microstructure. Based on observations of the cross-sectioned samples (Figure 3.22), it was found that there was no difference in grain size directly below the machined surface. Grain orientation appeared to be random, with no specific orientation resulting from machining. Comparisons between both machining techniques deeper within the material did not show any discernable difference in grain size and orientation. Overall, no significant difference was determined for the two types of machining when optically comparing microstructural cross-sections of the machined samples.

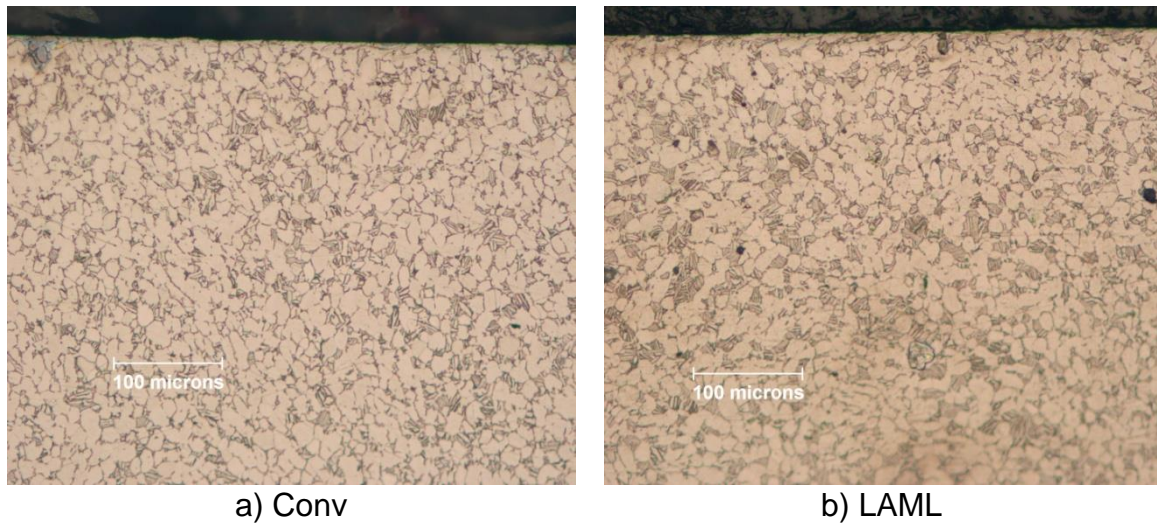


Figure 3.22: Ti-64 ELI Optical Microscope images from cross-sectioned samples etched with Kroll's reagent at 200x after traditional machining (a) and LAML (b).

SEM images of cross-sectioned samples were taken and compared between the traditional milling and LAML in order to evaluate grain size and orientation. Both the images showed a microstructure of equiaxed and distorted α , along with plate-like α , present with intergranular β through the entirety of the part. This is typical for a Ti-64 ELI grade 23 material that meets an AMS 4931 specification (Figure 3.23). By observing the cross-section of the material, it was found that there was not a significant change in composition from the top of the machined surface, all the way to the bulk of the material (2 mm deep). Ultimately, comparisons of optical microscope and SEM images indicated that the LAML process parameters did not result in a detrimental heat-affected zone for the final workpiece.

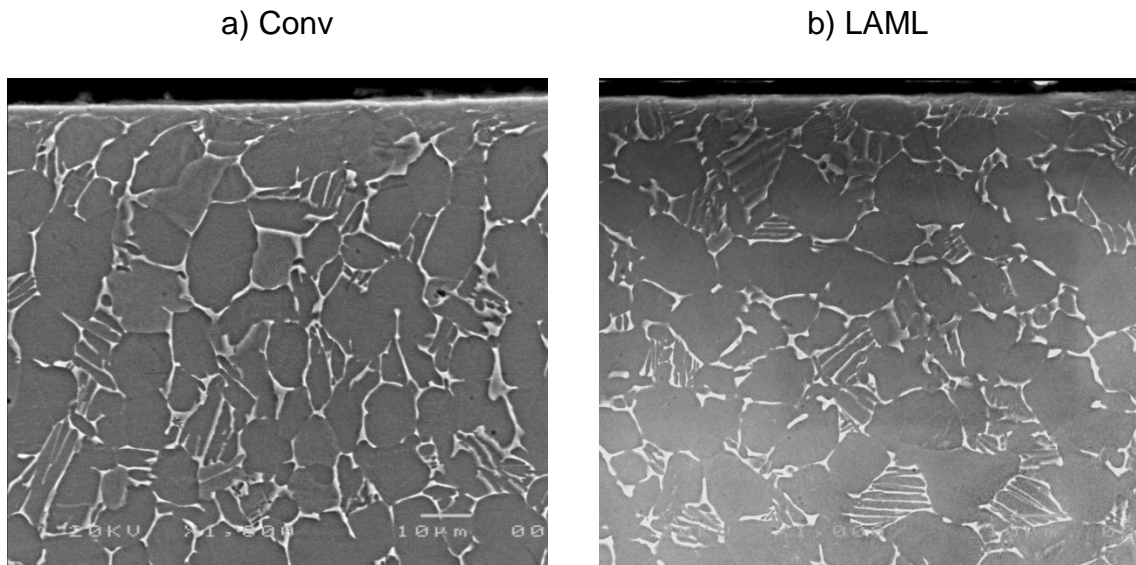


Figure 3.23: SEM Images of etched Ti-64 sample at 1,000x after traditional machining (a) and LAML (b).

Other studies have demonstrated that laser heating can be successfully applied to a Ti-64 alloy to change final part characteristics (Hahn et al., 2007). Although optical images and SEM images indicated that there was no significant microstructural change, XRD analysis was performed on the top workpiece surface to ensure that phase change was avoided for this critical area. Samples did not receive special preparation and had an average surface roughness of 0.3 μm . According to literature (Vreeling et al., 2002; Güleriyüz et al., 2004; da Silva et al., 1999), the standard way to characterize the 2θ peaks in Ti-64 is to use the JCPDS standard for titanium. The hexagonal α -Ti and cubic β -Ti from the JCPDS standard (file #44-1294, and #44-1288, respectively) were used in to determine where peaks should occur. This analysis is plotted along with the XRD experimental data (Figure 3.24).

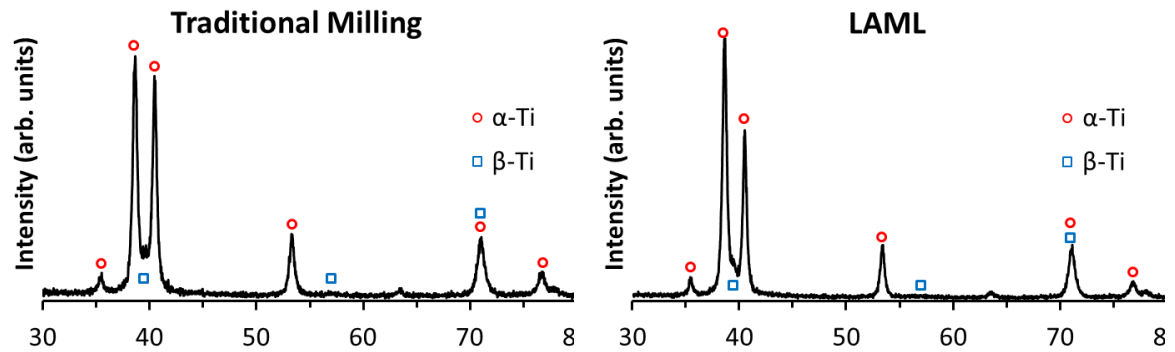


Figure 3.24: XRD analysis for milling Ti-64.

Based on a comparison of the peaks, the machined surface primarily consisted of α -phase Ti after traditional machining. Since there were no significant peaks present for the β -phase Ti on the LAML sample, it was concluded that machining with the laser did not induce a phase change, as long as accurate thermal modeling work was performed to determine an appropriate laser power. This conclusion was reinforced through the images from the SEM which showed no significant change in grain size and orientation through the cross-section. In examining this evidence, it can be concluded that initial thermal model predictions are accurate in determining laser parameters which enhance material removal without negatively affecting final part properties for a Ti-64 ELI heat-treatable workpiece.

A Mitutoyo hardness tester (model ATK F1000) was used to determine the surface hardness of the original Ti-64 ELI material, samples after traditional machining, and samples machined using LAML. Each sample was tested 7 times and the results are shown in Figure 3.25, where it can be seen that the final surface hardness of both traditional machining and LAML result in average

hardness values that are within the range of the as received material, as indicated by the error bars.

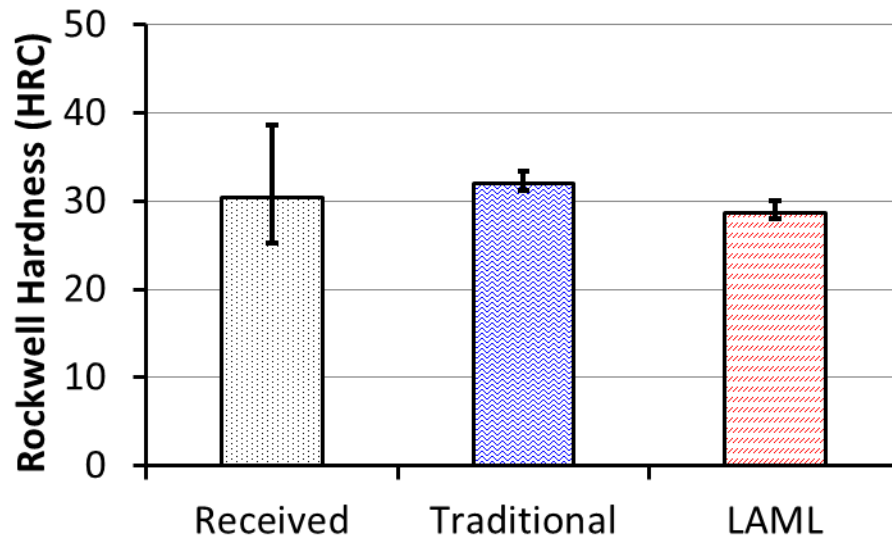


Figure 3.25: Ti-64 ELI surface hardness results for the as-received material, traditional milling at 50 m/min, and LAML at 75 m/min (error bars for the range of data).

The surface hardness tests indicate that there is a slight decrease in the surface hardness of the final part, but from the XRD analysis this was not a result of a detrimental phase change. An increase in surface hardness is common in traditional machining, due to grain size refinement and increased residual stresses. It has been shown that compressive residual stresses are generally observed during milling of titanium (Mantle and Aspinwall et al., 2001; Sun and Guo et al., 2009), which can induce a negative reduction of ductility on the part surface. The reduction in hardness is approximately 10% for the LAML samples

when compared with traditional machining, and the results of all machining were within the acceptable range based on the AMS 4931 specifications.

Due to the reduction in surface hardness found after LAML of the Ti-64 ELI workpiece, a detailed investigation into micro-hardness was performed along cross-sectioned parts to determine if there was a significant alteration in material composition beneath the surface. Microhardness tests were performed on samples for LAML at 75 m/min and traditional milling at 50 m/min. Microhardness was analyzed at intervals of 100 μm for each sample down to a depth of 2 mm. It was determined that there was a relatively consistent hardness for both LAML and traditional machining through the depth of the workpiece. A gradual increase in hardness was observed close to the surface of the workpiece for both LAML and traditional milling experiments. This indicates that the surface hardness differences measured are very shallow with respect to the top of the workpiece surface (Figure 3.26). It is significant to note that there was not a detrimental decrease in hardness of the workpiece as a result of LAML when compared with the bulk workpiece material.

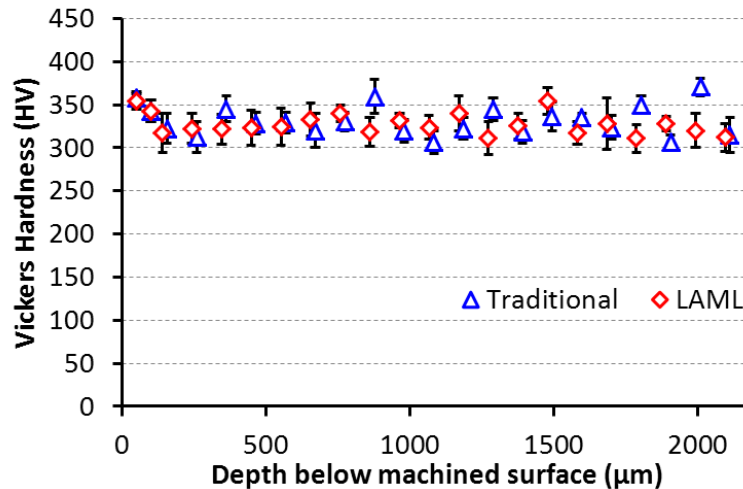


Figure 3.26: MicroHardness results for traditional machining at 50 m/min and LAML at 75 m/min.

Residual stress analysis was performed on the machined samples for traditional milling at 50 m/min and LAML at 75 m/min. Measurements were taken in the feed and machining direction down to a depth of 200 μm , where stresses returned to zero. A significant reduction in residual stress was not found in the machining direction for the two types of machining, with a difference being less than 8%. However, a reduction in residual stress of 25% was obtained for measurements of LAML in the feed direction when compared with traditional milling. For all residual stress measurements, compressive stress is present on the surface until the stresses return to zero. A comparison of residual stress data with respect to depth under the machined surface, for traditional milling and LAML, in the machining direction and feed direction for Ti-64 ELI is shown in Figure 3.27.

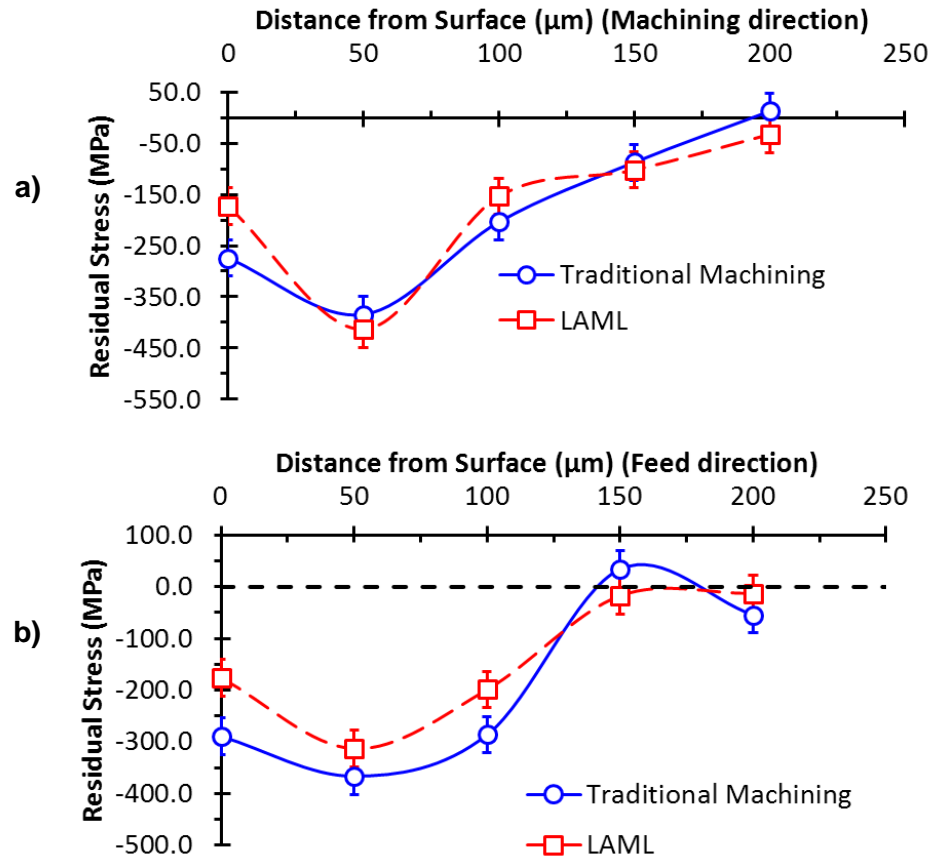


Figure 3.27: Residual Stress measurement for Ti-64 ELI after traditional machining at 50 m/min and LAML at 75 m/min for the machining direction (a) and feed direction (b).

Unlike the Ti-64 grade 5 residual stress results, there is not a clear indication that residual stresses are generally reduced for LAML machining of Ti-64 ELI in the machining direction. A 20% reduction in residual stress measured for LAML in the feed direction is apparent in Figure 3.27b when compared with traditional machining; however, similar results in the machining direction are not as clear. If all measurements are accurate, then the reduction in surface hardness is a result of the average reduction in residual stress in all directions.

As with the results for Ti-64 grade 5 machining, the changes to reduced residual stress only affects a very shallow portion of the machined workpiece and does not affect workpiece properties at deeper depths (below 200 μm). Final surface hardness measurements are closer to the bulk material hardness after LAML than with traditional milling. As a result of all of the microstructural analysis performed on the final workpiece, it can be concluded that LAML can be performed without negatively impacting final workpiece properties.

3.2.3 Economic Analysis

Because of the increase in tool life that can be achieved with LAML, a comparative cost savings was calculated for the Ti-64 ELI alloy for LAML and traditional machining. This analysis uses the following assumptions:

- \$200 per hour operation cost rate
- 3 min tool change time
- Tool cost: \$17 per insert – 2 cutting sides (\$8.50 per tip)
- Part size: 4,000 mm^3 (amount of material removed per part)
- At least one part made per tool
- Laser costs: \$30 per hour for operation & depreciation

Based on the given assumptions and the Taylor tool life equations obtained from experimental testing, the total cost per piece was plotted for different cutting speeds during traditional machining with a coolant and LAML (Figure 3.28). The cutting speed limitation of 50 m/min during traditional machining does not produce the minimum cost per part, but must be used in

industry to prevent premature chipping and potential damage to parts during machining. Since such chipping does not occur during LAML, higher speeds are possible for part fabrication. As a result, costs per part for LAML can be performed at speeds that are optimized based on total machining costs.

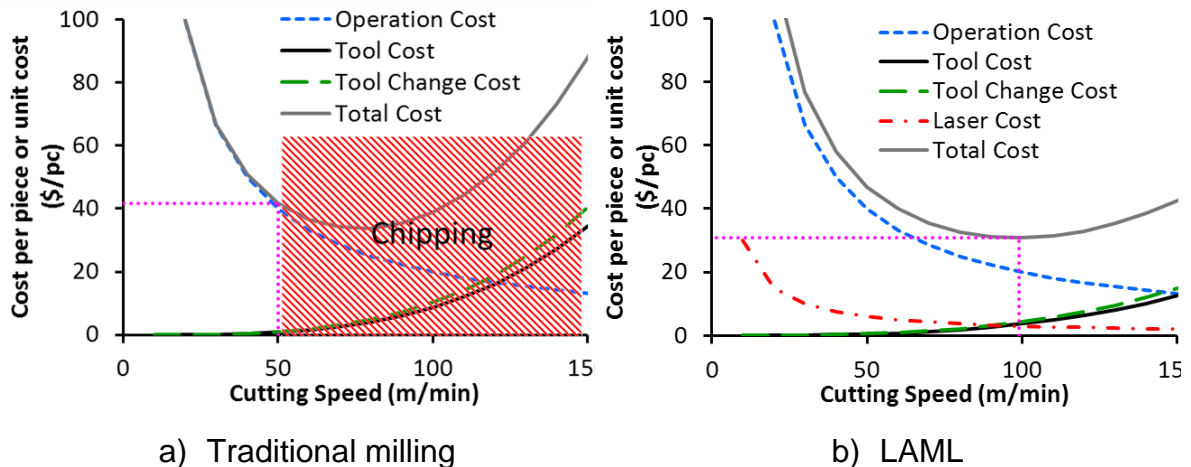


Figure 3.28: Cost of producing one part based on Taylor tool life equations.

The optimum cutting speed to minimize the total cost per part and maximize productivity of the machining center was determined for both traditional machining and LAML based on the experimental machining and laser parameters (Table 3.10). The increase from current traditional machining speeds of 50 m/min to 100 and 110 m/min for LAML indicated a significant increase in material removal and total production rate of parts. There was also a 30% reduction in cost per part when using LAML compared with traditional milling.

Table 3.10: Optimized cutting speed based on Taylor tool life equations – Ti-64 ELI milling.

Machining Type	Optimized cutting speed	
	Min-cost (m/min)	Max-productivity (m/min)
Conv	50	50
LAM	100	110

The total machining cost for cutting one piece is shown in Figure 3.29, with costs separated into their source (laser, tool change, tool cost, operational cost). Optimum cutting speeds were used for both LAML and traditional milling to calculate the minimum cost and maximum productivity. As evidenced in Figure 3.29, there is a 33% reduction in cost for producing parts using LAML, even when taking into accounting for costs of the laser operation.

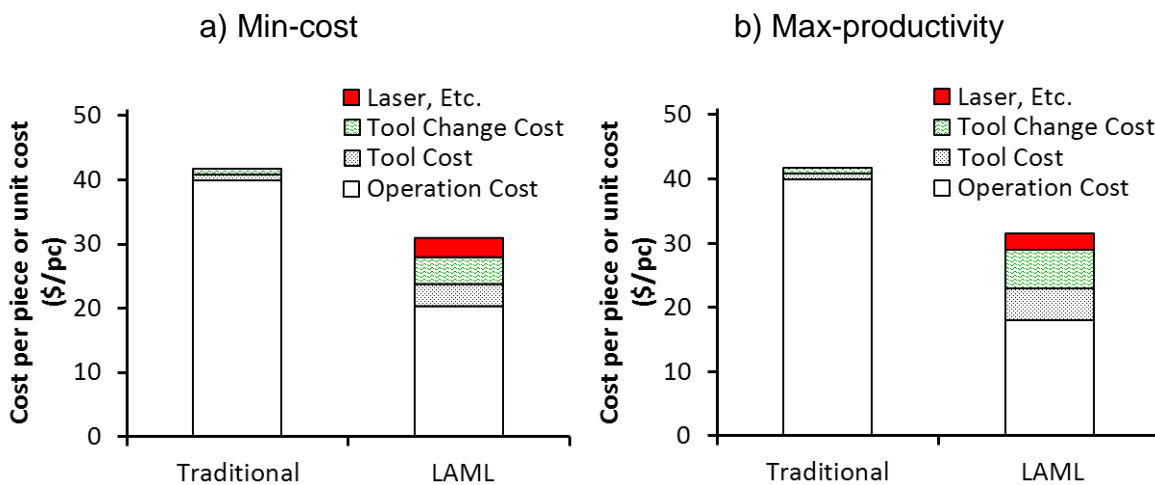


Figure 3.29: Economic Summary for optimized cutting conditions – Ti-64 ELI machining.

Because increases in cutting speed result in decreased total tool life, there is a larger percentage of cost per part that results from tool costs. However, it is

clear that LAML creates a significant improvement in both cost savings and production rate, despite the additional costs associated with the laser equipment and tool costs. It is important to note that results from this analysis are based on the tool life equations calculated from a lower flank wear criteria, as well as non-optimized machining and laser parameters. As a result, care must be used when directly applying these results to a specific industrial application. It is also noted that the LAML tool life test was completed only up to 100 m/min and tool life was estimated beyond 100 m/min using the established Taylor tool life equation.

As was indicated in the economic analysis of the Ti-64 grade 5 material, the benefits of eliminating a coolant were not included in Ti-64 ELI grade 23. One significant benefit of LAML over traditional milling, which is not considered in this economic analysis, is the impact of a coolant during machining. Since LAML does not require traditional coolants during the machining process, there can be added economic savings. There is also a direct environmental impact from the elimination of coolants since they do not need to be processed after use.

CHAPTER 4. LASER-ASSISTED MILLING – COMPLEX CONTOURING

4.1 System Design

For intricate shapes, additional complexities arise in keeping the laser beam coordinated with the cutting tool. One way to easily integrate a laser into a milling machine results in a setup with a fixed laser position relative to the machining axes. Such systems are only capable of performing machining passes in one direction. Although this initially limits the geometries that can be machined on a part, additional engineering solutions are available to overcome this drawback, and allow for the machining of more complicated shapes. For the work performed in this study, a 4th axis was integrated into the MAZAK machine. This added the functionality of rotation of the workpiece during milling, in addition to X and Y directional movement. As a result, the laser and milling system were able to machine complex contours onto a workpiece, while the laser remained stationary relative to the cutting tool.

4.2 System Integration and Experimental Setup

4.2.1 System Integration

For the MAZAK milling machine, a 4th axis was integrated to perform complex contouring. Control software was created to coordinate all axes of the

machine and the laser. A Troyke 9 inch diameter horizontal/vertical fourth axis rotary table driven by a Yaskawa 850 W, 200 V motor with a Yaskawa Sigma-5 1 kW, 200V motor driver was added to allow cutting of angles and contours. Tool paths were written in G&M code and converted to cubic spline coefficients by custom-made command generation software. Coordination of the turntable and MAZAK axes was then achieved through the open architecture controller (OAC) running on a National Instruments PXI-8176 controller with LabWindows RealTime operating system. Digital input and output were handled by two National Instruments PXI-6508 digital I/O, 96 line, 5 V TTL boards.

Communication between the OAC, the MAZAK, and the turntable was handled by an Altera UP2 field-programmable gate array (FPGA) programmed in the Quartus II 9.0 environment. The FPGA was connected to the OAC and to the MAZAK through custom-built printed circuit boards. This hardware setup is shown in Figure 4.1.

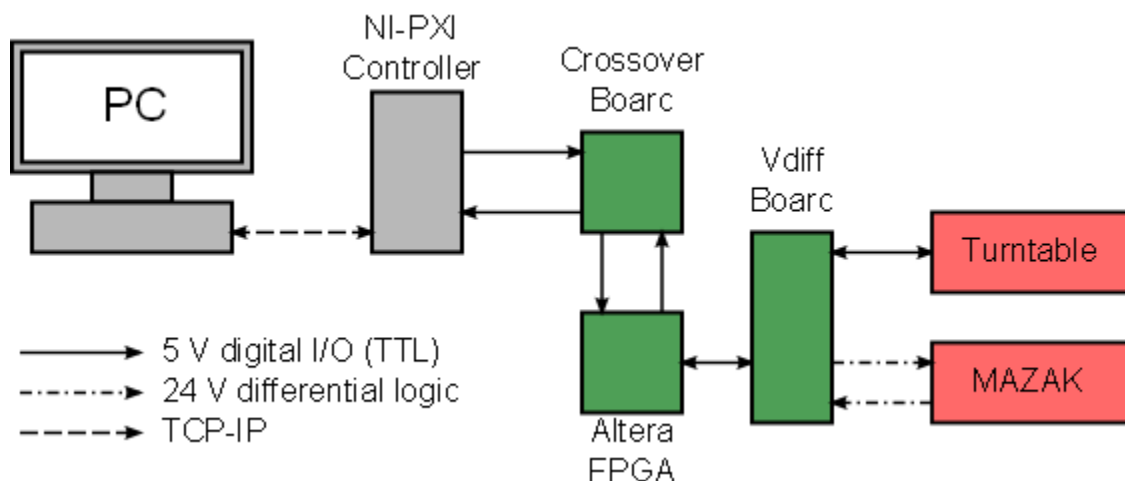


Figure 4.1: 4-Axis OAC hardware layout.

4.2.2 Experimental Setup

Experiments were completed using the MAZAK and Turntable to demonstrate the feasibility of LAML with complex contouring. A workpiece was held in position on the rotary table, and all machined paths were made in the x-direction, based on the dynamometer frame of reference discussed previously in this work. The workpiece was machined along two edges, using a 90° rotation in the middle of the process. Laser power was stopped during the repositioning interval as the laser moved off the workpiece surface.

For each full pass, a total of 220 mm of material was removed from the workpiece. Three full passes were performed using traditional machining and LAML. Each insert was removed after a total of 440 mm of material was removed, and tool wear was then recorded. A schematic of the contouring path is shown in Figure 4.2, and a list of machining parameters used is listed in Table 4.1.

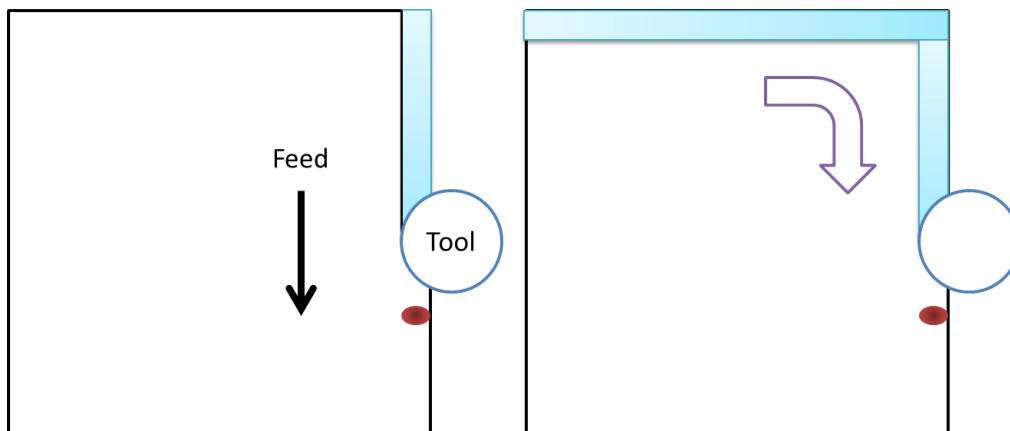


Figure 4.2: LAML Contouring Path for Experiments with One Direction Machining.

Table 4.1: Experimental Design for Complex Contouring Tests.

Test	Material	Doc (mm)	Woc (mm)	F (mm/s)	V (m/min)	RPM	L _{lead} (mm)	L _{spot} (mm)	P(W)
C-1	Grade 5	1.0	3	2.1	75	1250	-	-	-
CL-1	Grade 5	1.0	3	2.1	75	1250	3.0	2.6x3.5	180
C-2	ELI	1.0	3	2.1	75	1250	-	-	-
CL-2	ELI	1.0	3	2.1	75	1250	3.0	2.6x3.5	180

4.3 Experimental Results

From the results of the complex contouring, there was less tool wear for parts machined using LAML compared with traditional methods. Measured flank wear for the Ti-64 grade 5 machined paths were 101 μm for traditional machining and 82 μm for LAML. An overall improvement of 20% was observed after only 440 mm has been cut along the workpiece. Measured flank wear for the Ti-64 ELI grade 23 machined paths were 75 μm for traditional machining and 80 μm for LAML. Although an overall improvement of LAML was not observed for the length of cut performed on the ELI material, the general tool life follows the trend observed during typical machining. During Ti-64 milling using conventional and LAML, there was very little difference between overall flank wear rate during machining; however, premature failure of the tool was eliminated for the LAML case. It can be inferred from tool life results that although LAML does not significantly improve tool wear rate, complex contouring can be successfully implemented to improve total tool life when machining Ti-64 ELI.

As a result of the complex contouring experimental results, it can be concluded that LAML of complex parts is a feasible option which does not significantly reduce the tool life improvement available from LAML. Solutions are available to overcome hardware constraints which can limit machining to only one direction, in order to produce more complex shapes. By using a 4th axis and software and hardware coordination of the milling machine systems and fiber laser, LAML was shown to create more complex shapes while still improving tool life.

CHAPTER 5. CONCLUSIONS AND RECOMMENDATIONS

5.1 Conclusions

The prismatic thermal model was used to accurately predict workpiece temperature during the laser-assisted machining process when machining two Ti alloys, Ti-64 grade 5 and Ti-64 ELI grade 23. Modeling was performed to determine laser heating parameters, based on machining conditions during LAML, to ensure that a phase change was avoided during machining with a laser.

During milling of Ti-64, premature tool chipping dominated at machining speeds higher than 50 m/min. This study demonstrated that this random failure can be eliminated during LAML when using a proper laser power. As a result, higher machining speeds could be used without the premature tool chipping that can result in random tool failure. In addition to elimination of chipping, slower flank wear progression was demonstrated during tool life testing. The decrease in tool wear rate is a significant benefit to LAML over traditional machining, and shows the applicability of thermally-assisted machining to heat-treatable alloys.

Experimental data showed that for the Ti-64 grade 5 material, cutting speed could be increased by 35% while maintaining an equivalent tool life for traditional milling and LAML. For the Ti-64 ELI grade 23 alloy, tool life was improved by 64% when LAML was used instead of traditional milling. When a

constant tool life was employed, a 30% improvement in cutting speed was attained when using LAML. This improvement in cutting speed for both alloys is only feasible due to the elimination of premature chipping that occurs at higher cutting speeds during Ti-64 alloy machining using traditional milling.

From the results of optical microscopy and SEM images, it was determined that laser parameters obtained during modeling could be successfully employed to prevent a heat-affected zone from appearing on the workpiece during LAML. From XRD analysis, it was verified that a phase change was avoided on the top surface of the workpiece. Hardness testing indicated that LAML resulted in a slight decrease in surface hardness, but that the final hardness was within the range specified by the AMS standard for the respective materials. Additionally, after LAML, residual stresses were reduced by 10%, which closely matched the reduction in hardness for the workpiece surface. This reduction was limited to the top 200 μ m of the workpiece surface.

It was determined through the economic analysis that cost improvements and cutting speed increases can be achieved during the LAML process. The main economic benefit of LAML over traditional machining includes a 33% reduction in cost for both Ti-64 grade 5 and Ti-64 ELI grade 23. As a result of the elimination of tool chipping at high cutting speeds, LAML can also be performed at higher machining speeds than traditional milling. As a result, it was determined that LAML could produce two parts during the time it would take for one part to be produced during traditional milling of a Ti-64 grade 5 workpiece, and is achieved at the reduced economic cost of 33%.

The complex contouring feasibility experiments demonstrated the applicability of LAML to general milling operations which require complex geometry. Overall improvement of flank wear during machining was shown during complex contouring. This was determined by comparing flank wear that had occurred after a specified amount of machining time had taken place. From the complex contouring, results found a 20% improvement in flank wear for Ti-64 grade 5 machining after the specified amount of material had been removed. For Ti-64 ELI grade 23 complex contouring, the amount of material removed did not result in a significant improvement in tool wear when comparing traditional machining with LAML; however, it is expected that the elimination of chipping that was observed during the tool life experiments will be present during complex machining.

5.2 Recommendations

There is a clear improvement when using LAML during Ti-64 machining over traditional techniques. Laser and machining parameters that were used during LAML of Ti-64 were based on settings and tools designed for traditional milling. As a result, it is recommended that an investigation into cutting tool geometry be performed for LAML to determine if such modifications can further improve machinability. Additionally, further optimization of laser parameters may be performed to improve the LAML process for a Ti-64 alloy.

From tool life testing performed with the two different inserts (KC520 and KC725M) on the two Ti-64 alloys, it was determined that there is a difference in

overall tool life for the two different types of tools. Due to confounding of alloy type with tool type, it is unclear which tool provides a greater improvement for titanium parts machined using LAML. Further investigation is needed to determine which insert material offers the greatest improvement to LAML when machining Ti-64 alloys.

Complex contouring was successfully implemented. Additional testing should be conducted to determine optimum ways of applying the laser over complex shapes and the influence of laser power and Ramp up/Ramp down when the tool enters and exits the workpiece. Potential testing may also include how changing specific machining parameters influences surface integrity during complex contouring using LAML.

One of the initial assumptions made during this work was that a phase change is to be avoided after the material has been machined. However, roughing is typically not as sensitive to such changes, as additional material removal will occur after this process. Therefore, additional study is recommended to investigate the influence of higher laser power during LAML of Ti-64 alloys and the influence on cutting force and total tool life.

LIST OF REFERENCES

LIST OF REFERENCES

- Air Force Materials Laboratory (U.S.), Metals and Ceramics Information Center (U.S.), 1972, Titanium Alloys Handbook. Columbus, Ohio Metals and Ceramics Information Center.
- Amin, A. K. M. N., Ismail, A. F., and Nor Khairusshima, M. K., 2007, "Effectiveness of uncoated WC-Co and PCD inserts in end milling of titanium alloy—Ti-6Al-4V," *Journal of Materials Processing Technology*, Vol. 192-193(0), pp. 147-158.
- Anderson, M., Patwa, R., and Shin, Y.C., 2006, "Laser-assisted Machining of Inconel 718 with an Economic Analysis," *International Journal of Machine Tools and Manufacture*, Vol. 46, pp. 1879-1891.
- Bass, M., Beck, D., and Copley, S. M., 1978, "Laser assisted machining," *SPIE 4th European Electro-Optics Conference*, Vol. 164, pp. 233-240.
- Brecher, C., Rosen, C., Emonts, M., 2010, "Laser-assisted milling of advanced materials," *Physics Procedia*, Vol. 5(B), pp. 259-272.
- Chandler, H. W., 1989, *Machining of Reactive Metals. ASM Handbook – Machining*, vol. 10, pp. 844-857.
- Che Haron, C. H., Ginting, A., Arshad, H., 2007, "Performance of alloyed uncoated and CVD-coated carbide tools in dry milling of titanium alloy Ti-6242S," *Journal of Materials Processing Technology*, Vol. 185 (1-3), pp. 77-82.
- Cline, H. E. and Anthony, T. R., 1977, "Heat treating and melting materials with a scanning laser or electron beam," *Journal of Applied Physics*, Vol. 48, pp. 3895-3900.
- Dandekar, C. R., Shin, Y. C., Barnes, J., 2010, "Machinability improvement of titanium alloy (Ti-6Al-4V) via LAM and hybrid machining," *International Journal of Machine Tools and Manufacture*, Vol. 50(2), pp. 174-182.

- Ding, H., Shen, N., and Shin, Y. C., 2012, "Thermal and mechanical modeling analysis of laser-assisted micro-milling of difficult-to-machine alloys," *Micro-Manufacturing Processes*, Vol. 212(3), pp. 601-613.
- Güteryüz, H., and Çimenoğlu, H., 2004, "Effect of thermal oxidation on corrosion and corrosion–wear behaviour of a Ti–6Al–4V alloy," *Biomaterials*, Vol. 25(16), pp. 3325-3333.
- Hahn, J. D., 2006, "Laser assisted transformation hardening and nitriding of Ti-6AL-4V," Master thesis, Purdue University, West Lafayette IN.
- Hahn, J. D., Shin, Y. C., and Krane, M. J. M., 2007, "Laser transformation hardening of Ti–6Al–4V in solid state with accompanying kinetic model," *Surface Engineering*, Vol. 23 (2), pp. 78-82.
- Hong, S. Y., Markus, I., Jeong, W., 2001, "New cooling approach and tool life improvement in cryogenic machining of titanium alloy Ti-6Al-4V," *International Journal of Machine Tools and Manufacture*, Vol. 41(15), pp. 2245–2260.
- Jau, B. M., Copley, S. M. and Bass, M., 1980, "Laser assisted machining," *SME Technical Paper #MR80-846*, pp. 1-15.
- Jawaid, A., Sharif, S., and Koksai, S., 2000, "Evaluation of wear mechanisms of coated carbide tools when face milling titanium alloy," *Journal of Materials Processing Technology*, Vol. 99(1–3), pp. 266-274.
- Konig, W., and Zaboklicki, A. K., 1993, "Laser-assisted hot machining of ceramics and composite materials," *NIST Special Publication*, No. 847, pp. 455-463.
- Kovacevic, R., Cherukuthota, C., Mazurkiewicz, M., 1995, "High pressure waterjet cooling/lubrication to improve machining efficiency in milling," *International Journal of Machine Tools and Manufacture*, Vol. 35(10), pp. 1459–1473
- Kuljanic, E., Fioretti, M., Beltrame, L., and Miani, F., 1998, "Milling Titanium Compressor Blades with PCD Cutter," *CIRP Annals - Manufacturing Technology*, Vol. 47(1), pp. 61-64.
- Lei, S., Shin, Y. C., Incropera, F. P., 2001, "Experimental Investigation of Thermo-Mechanical Characteristics in Laser-Assisted Machining of Silicon Nitride Ceramics," *Journal of Manufacturing Science and Engineering*, Vol. 123 (4), pp. 639-646.

- Lindeke, R. R., Schönig, F. C., Khan, A. K., Haddad, J., 1991, "Machining of α -beta titanium with ultra-high pressure through the insert lubrication/cooling," Transactions of NAMRI/SME, Vol. 19, pp 154-161
- López de Lacalle, L. N., Pérez, J., Llorente, J. I., Sánchez, J. A., 2000, "Advanced cutting conditions for the milling of aeronautical alloys," Journal of Materials Processing Technology, Vol. 100 (1-3), pp. 1-11.
- Leshock, C. E., Kim, J., and Shin, Y. C., 2000, "Plasma enhanced machining of Inconel 718: modeling of workpiece temperature with plasma heating and experimental results," International Journal of Machine Tools and Manufacture, Vol. 41, pp. 877-897.
- Madore, C., Piotrowski, O., and Landolt, D., 1999, "Through-Mask Electrochemical Micromachining of Titanium," Journal of the Electrochemical Society, Vol. 146, pp. 2526-2532.
- Mantle, A. L., and Aspinwall, D. K., 2001, "Surface integrity of a high speed milled gamma titanium aluminide," Journal of Materials Processing Technology, Vol. 118, pp. 143-150.
- Novak, J. W., Shin, Y. C., and Incropera, F. P., 1994, "Assessment of plasma enhanced machining for improved machinability of Inconel 718," ASME, Production Engineering Division (PED), Vol. 68(1), Manufacturing Science and Engineering, pp. 443-451.
- Ozel, T., and Ulutan, D., 2012, "Prediction of machining induced residual stresses in turning of titanium and nickel based alloys with experiments and finite element simulations," CIRP Annals - Manufacturing Technology, Vol. 61, pp. 547-550.
- Pfefferkorn, F. E., Lei, S., Jeon, Y., Haddad, G., 2009, "A metric for defining the energy efficiency of thermally assisted machining," International Journal of Machine Tools and Manufacture, Vol. 49(5), pp. 357-365.
- Rajagopal, S., Plankenhorn, D. J., and Hill, V. L., 1982, "Machining aerospace alloys with the aid of a 15kW laser," Journal of Applied Metalworking, Vol. 2(3), pp. 170-184.
- Rao, B., Dandekar, C. R., Shin, Y. C., 2011, "An experimental and numerical study on the face milling of Ti-6Al-4V alloy: Tool performance and surface integrity," Journal of Materials Processing Technology, Vol. 211, pp. 294-304.

- Rahman Rashid, R. A., Bermingham, M. J., Sun, S., Wanga, G., Dargusch, M. S., 2012, "The response of the high strength Ti-10V-2Fe-3Al beta titanium alloy to laser assisted cutting," *Precision Engineering*, Vol. 37, pp. 461-472.
- Rozzi, J. C., Incropera, F. P., and Shin, Y. C., 1997, "Transient, three-dimensional heat transfer model for the laser assisted machining of ceramic materials," *Proceedings of the ASME International Mechanical Engineering Congress and Exposition*, Dallas, Tx, Vol. 351, pp. 75-85.
- Rozzi, J., Pfefferkorn, F., Shin, Y., and Incropera, F., 1998, "Transient thermal response of a rotating cylindrical silicon nitride workpiece subjected to a translating laser heat source: Part I-comparison of surface temperature measurements with theoretical results," *Transactions of the ASME: Journal of Heat Transfer*, Vol. 120, No. 4, pp. 899-906.
- Rozzi, J., Pfefferkorn, F., Shin, Y., and Incropera, F., 2000, "Transient, three-dimensional heat transfer model for the laser-assisted machining of silicon nitride: I: comparison predictions with measured surface temperature histories," *International Journal of Heat and Mass Transfer*, Vol. 43, pp. 1409-1424.
- Shelton, J. A., and Shin, Y. C., 2010a, "Laser-assisted micro-milling of difficult-to-machine materials in a side cutting configuration," *Journal of Micromechanics and Microengineering*, Vol. 20, pp. 075012.
- Shelton, J. A., and Shin, Y. C., 2010b, "Experimental evaluation of laser-assisted micro-milling in a slotting configuration," *Transactions of the ASME, Journal of Manufacturing Science and Engineering*, Vol. 132(2), pp. 021008.
- da Silva, S. L. R., Kerber, L. O., Amaral, L., and dos Santos, C. A., 1999, "X-ray diffraction measurements of plasma-nitrided Ti-6Al-4V," *Surface and Coatings Technology*, Vol. 116-119(0), pp. 342-346.
- Su, Y., He, N., Li, L., and Li, X. L., 2006, "An experimental investigation of effects of cooling/lubrication conditions on tool wear in high-speed end milling of Ti-6Al-4V," *Wear*, Vol. 261(7-8), pp. 760-766.
- Sun, J., and Guo, Y. B., 2008, "A new multi-view approach to characterize 3D chip morphology and properties in end milling titanium Ti-6Al-4V," *International Journal of Machine Tools and Manufacture*, Vol. 48(12-13), pp. 1486-1494.

- Sun, J., and Guo, Y. B., 2009, "A comprehensive experimental study on surface integrity by end milling Ti-6Al-4V," *Journal of Materials Processing Technology*, Vol. 209(8), pp. 4036-4042.
- Sun, S., Brandt, M., Barnes, J. E., and Dargusch, M. S., 2011, "Experimental investigation of cutting forces and tool wear during laser-assisted milling of Ti-6Al-4V alloy," *Proceedings of the Institution of Mechanical Engineers, Part B: Journal of Engineering Manufacture*, Vol. 225 (9), pp. 1512-1527.
- Thomas, M., Turner, S., and Jackson, M., 2010, "Microstructural damage during high-speed milling of titanium alloys," *Scripta Materialia*, Vol. 62(5), pp. 250-253.
- Tian, Y., and Shin, Y. C., 2006, "Thermal modeling for laser-assisted machining of silicon nitride ceramics with complex features," *Transactions of the ASME, Journal of Manufacturing Science and Engineering*, Vol. 128, pp. 425-434.
- Touloukian, Y. S., 1970, *Thermophysical Properties Research Center, Purdue University, Thermophysical properties of matter; [the TPRC data series; a comprehensive compilation of data]*. IFI/Plenum, New York.
- Vosough, M., 2005, "Effect of high-pressure cooling on the residual stress in Ti-alloys during machining," PhD thesis, Luleå University of Technology.
- Vreeling, J. A., Ocelík, V., and De Hosson, J. T. M., 2002, "Ti-6Al-4V strengthened by laser melt injection of WCp particles," *Acta Materialia*, Vol. 50(19), pp. 4913-4924.
- Wan, M., Zhang, W.-H., and Yang, Y., 2011, "Phase width analysis of cutting forces considering bottom edge cutting and cutter runout calibration in flat end milling of titanium alloy," *Journal of Materials Processing Technology*, Vol. 211(11), pp. 1852-1863.
- Wiedenmann, R., Langhorst, M., and Zaeh, M. F., 2011, "Computerized optimization of the process parameters in laser-assisted milling," *Lasers in Manufacturing - Proceedings of the Sixth International WLT Conference on Lasers in Manufacturing*, Vol. 12(A), pp. 607-616.
- Wiedenmann, R., Liebl, S., and Zaeh, M. F., 2012, "Influencing factors and workpiece's microstructure in laser-assisted milling of titanium," *Laser Assisted Net shape Engineering 7 (LANE 2012)*, Vol. 39, pp. 265-276.

Yang, J., Sun, S., Brandt, M., Yan, W., 2010, "Experimental investigation and 3D finite element prediction of the heat affected zone during laser assisted machining of Ti6Al4V alloy," *Journal of Materials Processing Technology*, Vol. 210(15), pp. 2215-2222.

VITA

VITA

Gary Hedberg
School of Mechanical Engineering, Purdue University

Gary Kent Hedberg received his Bachelor of Science in Mechanical Engineering in April of 2010 from Brigham Young University in Provo, Utah. Beginning in August of 2010, he started his graduate studies in the School of Mechanical Engineering at Purdue University. His research interests include experimental analysis, temperature prediction, and material properties with an emphasis on thermally enhanced machining.